



1 The Capability of Sentinel-MSI (2A/2B) and Landsat-OLI (8/9) 2 for Seagrass and Algae Species Differentiation using Spectral 3 Reflectance

4 Abderrazak Bannari ¹, Thamer Salim Ali ² and Asma Abahussain ²

5 ¹Space Pix-Map International Inc., Gatineau (Québec) J8R 3R7, Canada. Email: abannari@bell.net

6 ²Department of Natural Resources and Environment, College of Graduate Studies, Arabian Gulf University, Manama,
7 Kingdom of Bahrain, P.O. Box: 26671, Tel: (973) 1723-9545; Fax: (973) 1723-9552.

8
9 Correspondence to: Abderrazak Bannari, Email: abannari@bell.net

10

11 **Abstract.** This paper assesses the reflectance difference values between the homologous visible and near-infrared
12 (VNIR) spectral bands of Sentinel-MSI-2A/2B and Landsat-OLI-8/9 sensors for seagrass, algae, and mixed species
13 discrimination and monitoring in a shallow marine environment southeastern of Bahrain in the Arabian Gulf. To
14 achieve these, a field survey was conducted to collect samples of seawater, underwater sediments, seagrass (*Halodule*
15 *uninebell.netrvis* and *Halophila stipulacea*) and algae (green and brown). As well, an experimental mode was
16 established in a Goniometric-Laboratory to simulate the marine environment, and spectral measurements were
17 performed using an ASD spectroradiometer over each separate and different case of seagrass and algae mixed species
18 at different coverage rate (0, 10, 30, 75, and 100%) considering the bottom sediments with clear and dark colors. All
19 measured spectra were analyzed and transformed using continuum-removed reflectance spectral (CRRS) approach to
20 assess spectral separability among separate or mixed species at varying coverage rates. Afterward, the spectra were
21 resampled and convolved in the solar-reflective spectral bands of MSI and OLI sensors and converted into water
22 vegetation indices (WVI) to investigate the potential of red, green, and blue bands for seagrass and algae species
23 discrimination. For comparison and sensor differences quantification, statistical fits ($p < 0.05$) were conducted
24 between reflectances in homologous bands and also between homologous WVI; as well as the coefficient of
25 determination (R^2) and root mean square difference (RMSD) were calculated. The results of spectral and CRRS
26 analyses highlighted the importance of the blue, green, and NIR wavelengths for seagrass and algae detection and
27 probable discrimination based on hyperspectral measurements. However, when resampled and convolved in MSI and
28 OLI bands, spectral information loses the specific and unique absorption features and becomes more generalized and
29 less precise. Therefore, relying on the multispectral bandwidth of MSI and OLI sensors, it is difficult or even
30 impossible to differentiate or to map seagrass and algae individually at the species level. Additionally, instead of the
31 red band, the integration of the blue or the green bands in WVI increases their discriminating power of submerged
32 aquatic vegetation (SAV), particularly Water Adjusted Vegetation Index (WAVI), Water Enhance Vegetation Index
33 (WEVI), and Water Transformed Vegetation Index (WTDVI) indices. These results corroborate the spectral analysis
34 and the CRRS transformations that the blue and green electromagnetic radiation allows better marine
35 vegetation differentiation. However, despite the power of blue wavelength to penetrate deeper into the water,
36 it also leads to a relative overestimation of dense SAV coverage due to the higher scattering in this part of the spectrum.



37 Furthermore, statistical fits between the reflectance in the VNIR homologous bands of SMI and OLI revealed excellent
38 linear relationships (R^2 of 0.999) with insignificant RMSD (≤ 0.0015). Important agreements ($0.63 \leq R^2 \leq 0.96$) were
39 also obtained between homologous WVI regardless of the integrated spectral bands (i.e., red, green, and blue), yielding
40 insignificant RMSD (≤ 0.01). Accordingly, these results pointed out that MSI and OLI sensors are spectrally similar,
41 and their data can be used jointly to monitor accurately the spatial distribution of SAV and its dynamic in time and
42 space in shallow marine environment, provided that rigorous data pre-processing issues are addressed.

43 1. Introduction

44 Seagrass meadows are identified as an important key for the characterization of environmental resources in estuarine
45 and shallow coastal areas, and a fundamental health index allowing the assessment of coastal ecosystems. The
46 composition and density of their species depend largely on water depth, temperature, salinity, coastal substrate
47 material, and light penetration (Dierssen *et al.*, 2015). Adapted to grow in shallow seawater down to a depth of 20 m,
48 where approximately only 11% of surface light reaches the bottom (Duarte and Gattuso, 2008), they play an essential
49 role in the sustainability of global ecosystem biodiversity in most shallow near-shore areas around the world (Den-
50 Hartog, 1970; Konstantinos *et al.*, 2016). Moreover, the biodiversity of seagrass provides secure habitat and food for
51 a wide variety of marine micro-organisms, improve the quality of water and protect shorelines against erosion in the
52 middle and lower intertidal and sub-tidal zones (Roelfsema *et al.*, 2009; Anders and Lina, 2011; Yang and Yang,
53 2012; Morrison *et al.*, 2014). Like other vegetation cover, seagrass beds play an important role in carbon storage
54 (Novak and Short, 2020), as well as effective removal of carbon dioxide from the “biosphere-atmosphere” system,
55 which significantly mitigates the climate change impacts (Duarte *et al.*, 2013; Lyimo, 2016). Although occupying only
56 0.2% of the world’s oceans (Traganos, 2020), seagrass beds can store twice as much as forests, and
57 sequester around 10% of the total carbon received by the oceans (Fourqurean *et al.*, 2012).

58 Unfortunately, natural and anthropogenic disturbances and disasters have led to the decline of seagrass around the
59 world (Green and Short, 2003; Orth *et al.*, 2006; Grech *et al.*, 2012; Wood, 2012) at local and regional scales.
60 Undoubtedly, these causes substantially destroy the seagrass beds and biota associated in such habitat and unbalance
61 the ecological functions of coastal zones. Short *et al.* (2011) showed that seagrass habitat disappeared worldwide at a
62 rate of 110 km² per year between 1980 and 2006. Hence, understanding the spatial distribution of seagrass biomass,
63 its extent, condition, and change over time is essential for their monitoring, management, and protection (Short and
64 Coles, 2001; Waycott *et al.*, 2009). Such monitoring provides updated and accurate information useful for the
65 protection of several ecosystems (Leleu *et al.*, 2012), conservation (Hamel and Andréfouët, 2010), coastal risk
66 assessment (Warren *et al.*, 2016), ecological resources development (Boström *et al.*, 2011), and marine spatial
67 planning (Saarman *et al.*, 2012; Kibele, 2017). In addition, mapping and inventorying the total aboveground biomass
68 of seagrass and algae are important for ecosystem health assessment (Short and Wyllie-Echeverria, 1996), alteration
69 and dynamics in space-time (Neckles *et al.*, 2012), biomass productivity and its contribution to the global biosphere
70 carbon sink capacity (Waycott *et al.*, 2009), and understanding the impacts of climate change (Hashim *et al.*, 2014).



71 In the Arabian Gulf, the extreme environmental conditions combined with major seasonal variations in the marine
72 environment promote the development of three seagrass species including *Halodule uninervis* which is the most
73 dominant species, *Halophila stipulacea* that is less common, and *Halophila ovalis*, which is widely scattered and
74 rarely forms relatively dense meadows. Along the western coast of the Arabian Gulf, these three species are reported
75 and several species of marine algae are described, especially green and brown algae (Ertfemeijer and Shuail, 2012).
76 This natural resource is located in shallow waters with depths ranging from the intertidal zone to 20 m, supporting the
77 second largest population of dugongs (*Dugong dugon*) in the world (Preen, 2004); as well as a large population of
78 Green Turtles (*Chelonia mydas*) and Hawksbill Turtles (*Eretmochelys imbricata*) (Thakur et al., 2007). Unfortunately,
79 these coastal ecosystems are under continuous threats from anthropogenic activities (Waycott et al., 2009), such as
80 reclamation and dredging where several coastal developmental projects are constructed and others under construction
81 (small islands projects development), industrial effluents, oil exploration, pipeline laying, maritime transportation,
82 intensive circulation of commercial fishing boats, pollution and discharges of seawater desalination and wastewater
83 into the sea (Onuf, 1994; Dunton and Schonberg, 2002; Burfeind and Stunz, 2006; Humood, 2011; Ertfemeijer and
84 Shuail, 2012). Eventually, these activities catalyze the degradation and destruction of seagrass species and related
85 ecosystems. Therefore, the assessment of seagrass conditions associated with broad scale of benthic species should be
86 based on relevant and accurate information to measure several health indicators of coastal areas to ensure the
87 sustainable development of these natural resources.

88 Previously, photo-interpretation approaches based on aerial photography have been adopted to follow seagrass and
89 algae species development and assessment in space and time (Ferguson and Wood, 1990; Meehan et al., 2005; Mount,
90 2007). Afterward, the first generation of satellite remote sensing was used to investigate the seagrass classes'
91 composition, differentiation, classification, etc. (Ackleson and Klemas, 1987; Hossain et al., 2014; Komatsu et al.,
92 2020). Unfortunately, these goals were difficult to achieve accurately because the radiometric and spectral resolutions
93 of sensors lacked the sensitivity to discriminate among different marine vegetation species and fragmented classes
94 (Mumby et al., 1997; Wicaksono and Hafizt, 2013). To improve land-water surfaces reflectivity and information
95 extraction, recent developments in remote sensing science and technology have led to an improvement of sensors
96 performance in spatial and spectral resolutions, assuming a potential mapping of the marine environment and aquatic
97 vegetation at the species level; obviously, if species under investigation have distinct spectral signatures. For instance,
98 the Multi-Spectral Instruments (MSI) onboard Sentinel 2A and 2B, as well as the Operational Land Imager (OLI)
99 sensors onboard Landsat 8 and 9 platforms were designed with a significant improvement of the signal-to-noise ratio
100 (SNR) and radiometric performances (Knight and Kvaran, 2014). The availability of this new generation of sensors
101 offers innovative opportunities for long-term high-temporal frequency for Earth surfaces' observation and monitoring
102 (Mandanici and Bitelli, 2016). The free availability of their data significantly advances the applications of remote
103 sensing with medium spatial resolutions (Roy et al., 2014; Wulder et al., 2015; Zhang et al., 2018). Thanks to the
104 improvement of their spectral, radiometric, and temporal resolutions, they can expand the range of their applications
105 to several natural resources and environmental domains for monitoring, assessing, and investigating (Hedley et al.,
106 2012a and 2012b). Moreover, the orbits of these four satellites constellation are designed to ensure a revisiting interval
107 time of less than 2 days (Li and Roy, 2017; Li and Chen, 2020), thereby substantially increasing the monitoring



108 capabilities of the Earth's surface and ecosystems (Drusch et al., 2012). Their spectral resolutions and configurations
109 are designed in such a way that there is a significant match between the homologous spectral bands (Drusch et al.,
110 2012; Irons et al., 2012). However, depending on the sensitivity of the intended application (Flood, 2017), the sensor
111 radiometric drift calibration (Markham et al., 2016), the atmospheric corrections (Vermote et al., 2016), the surface
112 reflectance anisotropy (Roy et al., 2017), and the sensors co-registration (Skakun et al., 2017; Yan et al., 2018), it is
113 plausible that the natural surface-reflectances recorded by MSI and OLI sensors over the same target in the marine
114 environment may be different. In addition, the relative spectral response profiles characterizing the filters (spectral
115 responsivities) of these instruments are not perfectly identical between the homologous bands, so some differences
116 are probably expected over the recorded land or water surfaces reflectance values and, therefore, their data cannot be
117 reliably used together (Bannari et al., 2004; Van-derWerff and Van-der-Meer, 2016; Bannari, 2019). The importance
118 of these differences depends on the application (spectral characteristics of the observed target) and on the approach
119 adopted to perform time-series analyses, mapping, or change detection exploiting these instruments (Flood, 2017).
120 For instance, it is plausible that the extraction of seagrass and/or algae information in time over shallow water areas
121 using surface reflectances, empirical, semi-empirical, and/or physical approaches, may affect the comparison of the
122 results.

123 The main objectives of this research focus on the analysis of Sentinel-MSI and Landsat-OLI homologous visible
124 and near-infrared (VNIR) bands capability to distinguish and discriminate among seagrass (*Halodule uninervis* and
125 *Halophila stipulacea*), algae (green and brown), and any probable case of mixed species of seagrass and algae sampled
126 from the southeast area of Bahrain national water. To achieve these, the specific following steps are considered. 1)
127 Examination of spectral signatures in VNIR wavelengths and their continuum-removal transformations for potential
128 differentiation among the considered seagrass and algae species and their mixture submerged in seawater at different
129 coverage rates, as well as considering the sediment-substrate with clear and dark colors. 2) Comparison and analysis
130 of the difference between the resampled and convolved reflectances in the VNIR homologous bands of MSI and OLI
131 sensors considering all examined samples. 3) Comparison between MSI and OLI sensors in terms of converting the
132 reflectances over the considered samples at different coverage rates into several water vegetation indices (WVI).
133 Finally, 4) efficiency and accuracy analysis of the examined WVI to discriminate between species (seagrass, algae
134 and mixed) by integrating the green and blue bands instead of the red band. Further, according to these analyses
135 results, it will be clear whether it possible for these sensors to differentiate between seagrass and algae effectively and
136 precisely at the species level, or simply and generally to discriminate among submerged aquatic vegetation (SAV)
137 cover at different density classes.

138 2. Remote sensing of seagrass and algae detection and mapping: A review

139 Traditional seagrass *in-situ* surveys require time and intensive field sampling, which is generally lack the spatial
140 coverage and precision that are required to detect changes before they become irreversible or very difficult to maintain
141 year after year (Peterson and Fourqurean, 2001, Yang and Yang, 2012). Over the recent decades, remote sensing
142 science and sensors technology has played an essential role in seagrass mapping and monitoring (Dean and Salim,
143 2013; Dierssen et al., 2015). According to literature, the mapping of the characteristics and properties of seagrass and



144 algae in the marine environment occurs over relatively small areas with limited variations in water depth and clarity
145 using satellite, airborne, and drone remote sensing sensors (multispectral and hyperspectral). Moreover, field and
146 laboratory *in-situ* measurements have been conducted for calibration and validation in several environments around
147 the world (Larkum *et al.*, 2006; Roelfsema *et al.*, 2009; Hossain *et al.*, 2014; Komatsu *et al.*, 2020; Duffy *et al.* 2018).

148 Under laboratory conditions using spectral measurements, Thorhaug *et al.* (2007) demonstrated the near similarity
149 in the shape and form of the spectral signatures of three different seagrass species with a very slight difference and
150 pointed out subtle differences between marine algae (green and brown) and seagrass. In the central west coast of
151 Florida in the USA, Pu *et al.* (2012) used *in-situ* Hyperspectral measurements in the field and laboratory to analyse
152 the spectral behaviour and the potential discrimination among several seagrass species according to their spatial extent
153 and abundance, water depths, and substrate types. They highlighted that the discrimination of seagrass species and the
154 percentage of SAV coverage are affected by water depth and substrate on the measured spectra. Moreover, Wood
155 (2012) demonstrated the potential of the synergy between the field spectra and hyperspectral data for seagrass sensing
156 and mapping in Redfish Bay, Texas in the USA. Exploiting modeled and simulated data, Hedley *et al.* (2012a)
157 demonstrated that Sentinel-MSI has an improved capability for detection and discrimination of the marine
158 environment compared to SPOT-4 and Landsat-ETM+. Furthermore, Fyfe (2003) reported that the spectral signatures
159 measured on harvested wet leaves (out of water) of different seagrass species were spectrally distinct. However, the
160 real marine environment conditions are different from wet leaves due to water-column constituents including
161 phytoplankton, suspended organic and inorganic matter, water depth variability, and optical properties of the
162 underlying sediments (Pu *et al.*, 2012).

163 Otherwise, NASA's Landsat program is the earliest and most commonly used over the past five decades, it consists
164 of a series of nine satellite missions (1 to 9) using four types of multispectral sensors including MSS, TM, ETM+,
165 and OLI (Bannari and Al-Ali, 2020) which have been used by many scientists to detect and map seagrass beds at local
166 and regional scales (Ackleson and Klemas 1987; Luczkovich *et al.* 1993; Shapiro and Rohmann 2006; Phinn *et al.*
167 2008; Knudby and Nordlund, 2011; Lyons *et al.* 2012 and 2013; Kovacs *et al.* 2018). Exploring a time-series of 23
168 annual images acquired over the Eastern Banks of Moreton Bay in Australia, Lyons *et al.* (2013) demonstrated how
169 Landsat TM and ETM+ data time-series analysis enabled seagrass distribution to be appropriately assessed in the
170 context of its spatial and temporal history and provide the ability to not only quantify change but also describe the
171 type of change. Moreover, a regional-scale mapping of seagrass habitat in the Wider-Caribbean region was achieved
172 with acceptable accuracies using a total of 40 Landsat scenes acquired with TM and ETM+ sensors, and applying
173 different images processing methods, i.e., segmentation, contextual editing, supervised classifications, etc. (Wabnitz
174 *et al.*, 2008). In Cam-Ranh Bay in Vietnam, Chen *et al.* (2016) investigated the temporal changes of seagrass beds
175 over 20 years (1996 to 2015) by exploiting multi-temporal Landsat data acquired with TM, ETM+ and OLI sensors.
176 Dekker *et al.* (2005) demonstrated that Landsat TM and ETM+ instruments did not have sufficient spectral and
177 radiometric resolutions to discriminate among three seagrass species in a shallow coastal Australian lake.
178 Contrariwise, Dahdouh-Guebas *et al.* (1999) reported the utility of Landsat-TM data associated with ground truth
179 measurements to map accurately the distribution of seagrass and algae on the Kenyan coast. In addition to the Landsat
180 sensor series, the European satellites such as SPOT-HRV were also used in combination with *in-situ*



181 spectroradiometric measurements and quantitative semi-empirical models to assess the changes in the spatial
182 distribution of seagrass biomass in Bourgneuf-Bay in France over 14 years (Barillé et al. 2010). Likewise, the potential
183 of the Indian satellite (IRS-ID LISS-III) has been demonstrated for mapping the seagrass meadows extent in the Gulf
184 of Mannar Biosphere Reserve in India (Umamaheswari et al., 2009).

185 Furthermore, the first generation of commercial satellites operated by the private remote sensing industry with
186 very high pixel size and narrow spectral resolutions, such as IKONOS, Quickbird, WorldView, etc., offers
187 complementary technology for seagrass sensing and mapping. This new technology provides an excellent compromise
188 between spatial and spectral resolutions for information extraction. In clear water seagrass habitat in the Moreton-Bay
189 (Australia), the spatial and temporal dynamics of seagrasses (cover, species, and biomass) have been studied from the
190 leaf to patch scales between 2004 and 2013 integrating nine high spatial resolutions images acquired with WorldView-
191 2, IKONOS, and Quickbird-2 and applying object-image processing approach (Roelfsema et al., 2014). The results
192 showed the utility of this new high spatial technology for time-series analysis and the derivation of seagrass products
193 that are very useful in marine ecology management. Moreover, Knudby and Nordlund (2011) highlighted the utility
194 of IKONOS data for seagrass detection in a patchy multi-species environment around Chumbe Island in Zanzibar
195 (Tanzania). Along Zakynthos Island in Greece, Pasqualini et al. (2005) demonstrated that the SPOT-5 data with 2.5
196 and 10 m spatial resolutions are suitable for seagrass classes' classification according to the overall accuracies, but
197 the pixel size of 2.5 m provided lower accuracy than 10 m. In shallow waters of Moreton Bay in Australia, Phinn et
198 al. (2008) have shown that the spatial and spectral resolutions of multispectral (Quickbird and Landsat-TM) and
199 hyperspectral (airborne CASI) data affects the precision of seagrass biomass differentiation at the species level, i.e.,
200 when the pixel size increases the error is getting higher. Contrary to these findings, Dattola et al. (2018) reported the
201 potential of the high spatial resolution of WorldView-2 compared to the medium resolution of Sentinel-MSI and
202 Landsat-OLI for different seagrass species characterization in the Capo Rizzuto area in Italy. In addition, using
203 QuickBird, CBERS (China-Brazil Earth Resources Satellite data), and Landsat-TM data to identify the spatial
204 distribution of seagrass beds in Xincun Bay (Hainan province in China), Yang and Yang (2009) demonstrated that
205 Quickbird data are more accurate than those of TM and CBERS sensors.

206 In addition to remote sensing sensor technologies, a variety of image processing methods have been employed in
207 mapping seagrass spatial distribution and coverage. For instance, Marcello et al. (2018) demonstrated the good
208 performance of support vector machines (SVM) approach compared to spectral angle mapper (SAM) and maximum
209 likelihood for seagrass classification; moreover, they pointed out the greater aptitude of hyperspectral compared to
210 multispectral data. Likewise, Peneva et al. (2008) reported that the maximum likelihood classification produced the
211 highest overall accuracy while SAM yielded the lowest accuracy due to the predominant influence of water-column
212 optical properties on the apparent spectral characteristics of seagrass and sand bottom in the northern Gulf of Mexico.
213 For *Posidonia oceanica* mapping in the Mediterranean region, the random forests method gives more accurate results
214 than SVM approaches when compared with in-situ observations (Bakirman and Gumusay, 2020). Whereas, using a
215 high spatial resolution of WorldView-2 imagery acquired over a coastal area in Florida, the neural network classifier
216 performed better than SVM for seagrass mapping (Perez et al., 2020). According to Uhrin and Townsend (2016),
217 linear spectral mixture analysis (LSMA) can be used with photo interpretation to generate spatially resolved maps



218 suitable for seagrass spatial distribution and provide improved estimates of seagrass classes. Nevertheless, Chen et al.
219 (2016) revealed the difficulty and limitation of LSMA for mapping the fraction of scattered and heterogeneous
220 seagrass patches that are smaller than the pixel size. At Ritchie's archipelago within the Andaman and Nicobar group
221 of Islands, Bayyana et al. (2020) showed that Sentinel-MSI data can detect, and map submerged benthic habitat and
222 seagrass beds present at a depth of 21 m using random forest, SVM, and K-nearest-neighbour classification algorithms.
223 Besides, linear regressions were established between the field truth measurements and several vegetation indices
224 derived from SPOT-XS, Landsat-TM, and CASI Hyperspectral airborne, to measure the density of seagrass in the
225 tropical Western Atlantic (Mumby et al., 1997).

226 Since the emergence of remote sensing as a new scientific discipline in the early 1970s, vegetation indices (VI's)
227 were involved as radiometric measurements of the spatial and temporal distribution of land vegetation photo-
228 synthetically active. They use the red and near-infrared (NIR) bands, the normalized difference vegetation index
229 (NDVI) was proposed by Rouse et al. (1974) at the dawn of remote sensing. Since these two spectral bands are
230 generally present on Earth observation and meteorological satellites, and often containing more than 90% of the
231 information relating to vegetation canopy (Bannari et al., 1995), the NDVI had taken a privileged place in the
232 NASA/NOAA Pathfinder project (James and Kalluri, 1994). Thus, it was daily derived from NOAA-AVHRR data at
233 the Earth scale. Subsequently, it was also derived every day from MODIS and SPOT-Vegetation data to produce time-
234 series products for global vegetation assessment and monitoring at the regional and global scales. Due to this glorious
235 history and its simplicity, the NDVI has become the most widely used to assess vegetation canopy. Then, this index
236 was improved in a new version named soil adjusted vegetation index (SAVI) by Huete (1988) to minimize the artefacts
237 caused by soil background on the estimation of vegetation cover fraction by incorporating a correction factor "L". To
238 overcome the limitations of linearity and saturation, to reduce the noise of atmospheric effects, and to remove the
239 artefacts of soil optical properties, the enhanced vegetation index (EVI) was proposed also by Huete *et al.* (2002).
240 Likewise, the transformed difference vegetation index (TDVI) was developed by Bannari *et al.* (2002) to describe the
241 vegetation cover fraction independently to the background artefacts, to reduce the saturation problem, and to enhance
242 the vegetation dynamic range linearly. These indices (NDVI, SAVI, EVI, and TDVI) were used to establish a close
243 relationship between radiometric responses and land vegetative cover densities, and they were implemented in the
244 ENVI image processing system.

245 In marine applications, these indices were tested by several scientists for seagrass and algae discrimination and
246 mapping. For a spatiotemporal change in seagrass beds in Bourgneuf-Bay in France, the NDVI extracted from SPOT-
247 HRV images coupled with *in-situ* spectroradiometric data provided satisfactory results (Barillé et al., 2009). Using
248 hyperspectral data, Dierssen et al. (2015) reported the potential of NDVI for SAV classes' discrimination. Similarly,
249 Zoffoli et al. (2020) demonstrated the capability of NDVI derived from Sentinel-MSI data for seagrass percent cover
250 estimation and leaf biomass mapping to characterize its seasonal dynamics along the European Atlantic coast.
251 However, although VNIR bands are generally available in optical remote sensing satellites, it is well known that only
252 the visible bands can penetrate ocean water deeper than NIR which is largely absorbed by the water surface (Kirk,
253 1994). Thus, regardless of the concentrations of suspended sediments and/or organic matter, the visible wavelengths
254 are used to map the marine environment as the blue penetrates deeper (~ 37 m) than any other wavelengths, followed



255 by green (~ 30 m), then red (~ 7 m), and NIR (Fig. 1) penetrates the least, being attenuated in the shallowest depths
256 around 2.5 m (Komatsu et al., 2020). Accordingly, blue, green, and red are the most suitable for sensing seagrass and
257 SAV (Silva et al., 2008). Thereby, when vegetation indices are applied in the marine environment (Davranche et al.,
258 2010; Zhao et al., 2013), always the red band is substituted by that of blue or green. Then, discussion was initiated on
259 WVI or aquatic vegetation indices (AVI). For instance, when the red was replaced by the green in NDVI (Yang and
260 Yang, 2009) and by the blue in SAVI (Villa et al., 2013) these versions were named, respectively, the Normalized
261 Difference Aquatic Vegetation Index (NDAVI or WNDVI) and Water Adjusted Vegetation Index (WAVI). These
262 two new versions were found more sensitive to seagrass LAI and percentage cover density, and discriminated better
263 among species of seagrass (Yang and Yang, 2009; Villa et al., 2013). To separate and map vegetation features over
264 some lake ecosystems in Italy, the NDAVI and the WAVI performed suitably (Villa et al., 2014). As well, for open
265 water features delineation, Mcfeeters (1996) replaced the difference between “NIR and red” in the NDVI with that
266 between “green and NIR”, and he baptised this new combination the Normalized Difference Water Index (NDWI). In
267 Taihu and Duck Lakes in China, NDVI and NDWI were used for wetland and SAV pattern delineation and
268 classification (Lin et al., 2010; Zhao et al., 2013). Likewise, the visible atmospherically resistant index (VARI) was
269 proposed by Gitelson et al. (2002a) to estimate the green vegetation fraction. While the triangular greenness index
270 (TGI) was developed by Hunt et al. (2013) based on the chlorophyll absorption features. The capability of VARI and
271 TGI was examined by Li (2018) who highlighted the advantage of VARI compared to TGI for seagrass biomass
272 mapping in Core Banks in North Carolina in the USA. Proposed by Richardson and Wiegand (1977), the difference
273 vegetation index (DVI) provided satisfactory results for mangrove cover and carbon stock estimation in the estuary
274 and marine environment (Candra et al., 2016). Moreover, the difference-index between the blue and the green bands
275 (DIF-BG) showed the best fits between observed and predicted SAV as reported by Mumby et al. (1997).

276

277 [Figure 1]

278 3. Materials and Methods

279 Fig. 2 illustrates the followed methodology, which is based on a field survey to collect samples including seawater,
280 sediments, seagrass (*Halodule uninervis* and *Halophila stipulacea*) and algae (green and brown) from shallow marine
281 environment at different depths (0.50 to 7 m) of southeast Bahrain. To simulate the marine environment, an
282 experimental mode was established in a Goniometric-Laboratory and spectral measurements were performed using
283 an Analytical Spectral Devices (ASD) spectroradiometer over each separate and mixed species at different coverage
284 rate (0, 10, 30, 75, and 100%), as well as simulating the seabed with dark and clear colors. To assess the spectral
285 signatures variability that can be found among each separate or mixed species at varying coverage rates, all measured
286 spectra were analyzed and transformed using continuum-removed reflectance spectral (CRRS) approach (see section
287 3.4). Then, the spectra were resampled and convolved in the solar-reflective spectral bands of MSI and OLI sensors
288 using the *Canadian Modified Simulation of a Satellite Signal in the Solar Spectrum* (CAM5S) (Teillet and Santer,
289 1991) based on Herman radiative transfer code (RTC), and the relative spectral response profiles characterizing the
290 filters of each instrument in the VNIR bands. Afterward, convolved spectra were converted into several WVI



291 integrating the red, green, and blue bands. For comparison and sensor differences quantification, statistical fits were
292 conducted using linear regression analysis ($p < 0.05$) between reflectances in homologous bands and between the
293 examined homologous WVI derived from the two sensors data considering all samples, i.e., seawater, sediments,
294 seagrass, and algae species (individually and mixed at the considered coverage rates). The coefficient of determination
295 (R^2), difference values, and root mean square difference (RMSD) were calculated for reflectances and all versions of
296 investigated WVI's.

297

298

[Figure 2]

299 3.1. Study Site

300 The area under investigation in this research is the water boundary of the Kingdom of Bahrain (25° 32' and 26°00'N,
301 50° 20' and 50° 50'E) which is a group of islands located in the Arabian Gulf, east of Saudi Arabia and west of Qatar
302 (Fig. 3). The archipelago comprises 33 islands, with a total area of 8269 km², 9% of it is a land area (778.4 km²).
303 Along the southeast coast of Bahrain, the continental plateau extends for kilometers with a depth of less than one or
304 two meters. The main island of Bahrain is surrounded by shoal areas named “Fashts” where depths do not exceed 10
305 m (Bannar i and Kadhem, 2018). These areas generally support a variety of species of seagrass, algae, coral, and
306 fishes. Moreover, they play an important role in the hydrodynamic regime, which supports diverse biological
307 ecosystems. Fig. 3 also illustrates the reclamation and dredging operations that have occurred in the study area over
308 the past three decades where several coastal developmental projects are constructed, and others are in progress. These
309 anthropogenic activities strongly contribute to the degradation and even to the destruction of seagrass species and
310 associated coastal ecosystems.

311

312

[Figure 3]

313 3.2. Field sampling

314 Seagrass and algae samples were collected on 4th May 2017 from different meadows locations, which are characterized
315 by a depth range from 0.5 to 7 m in the south and southeast waters of Bahrain (Fig. 4a). Some locations were dominated
316 with *Halodule uninervis* (HU), others scattered, or dense patches were a mixture between HU and *Halophila*
317 *stipulacea* (HS). HU is the most dominant species (Fig. 4b), it occurs as dense or scattered meadows patches along
318 shoreline (Erftemeijer and Shail, 2012). This species is like grass with narrow leaves (around 3 mm in width and 25
319 cm in length). Whereas, HS (Fig. 4c) has darker green leaves reaching 10 cm in length and it is widely present in the
320 Arabian Gulf. The brown (BA, Fig. 4d) and green (GA, Fig. 4e) algae were accessible near to shores and shallow
321 water in general. In addition to the sediments (Fig. 4f) and pure seawater samples which were collected separately,
322 samples of each seagrass and algae species were selected and harvested in healthy and fresh conditions from several
323 stations within the study area, and then stored separately in non-translucent plastic bags with seawater and immediately
324 placed in a cooler for transportation from the field to the laboratory. This was done to prevent structural and leaf



325 pigment damages due to the delay between sampling time and spectroradiometric measurements in the Goniometric-
326 Laboratory.

327

328

[Figure 4]

329 3.3. Spectroradiometric measurements

330 Spectroradiometric measurements were acquired in a dark BRDF Goniometric-Laboratory above each separated and
331 mixed samples (Fig. 5) using an ASD spectroradiometer (ASD Inc., 2015). This instrument is equipped with two
332 detectors operating in the VNIR and shortwave-infrared (SWIR), between 350 and 2500 nm. It acquires a continuous
333 spectrum with a 1.4 nm sampling interval from 350 to 1000 nm and 2 nm from 1000 to 2500 nm. The ASD resamples
334 the measurements in 1-nm intervals, which allows the acquisition of 2151 contiguous hyperspectral bands per
335 spectrum. The sensor is characterized by the programming capacity of the integration time, which allows an increase
336 of the SNR and stability. The data were acquired at nadir with a field of view (FOV) of 25° and a solar zenith angle
337 of approximately 5° by averaging 40 measurements. The ASD was installed on a BRDF Goniometric-System with a
338 height of approximately 65 cm over the target, which makes it possible to observe a surface of ~ 830 cm². A laser
339 beam was used to locate the center of the ASD-FOV. The reflectance factor of each sample was calculated by rationing
340 target radiance to the radiance obtained from a calibrated “Spectralon panel” according to the method described by
341 Jackson et al. (1980). Moreover, the corrections were applied for the wavelength dependence and non-lambertian
342 behavior of the panel (Sandmeier et al., 1998; ASD, 2015; Ben-Dor et al., 2015). The measurements were carried out
343 above each collected sample including seawater, sediments, seagrass, and algae species as well as mixed species
344 (seagrass and algae) considering different coverage rates (0, 10, 30, 75, and 100%). Each sample was placed and
345 measured twice in black and clear-bright (yellow) large bowls, considering two sedimentary substrates (dark and clear-
346 bright) underlying the seagrass and algae samples that were submerged by seawater, i.e., simulating the aquatic
347 environment. Since the remote sensing of benthic aquatic vegetation is mostly limited to the VNIR ranges (Fig. 1)
348 only the wavelengths interval between 400 and 1000 nm are considered in our analyses.

349

350

[Figure 5]

351 3.4. Continuum-removed reflectance spectral (CRRS) transformation

352 Spectral signatures are processed and transformed using numerous approaches to retrieve information regarding the
353 change in reflectance of a particular target over a specific bandwidth between 350 and 2500 nm (Van-Der-Meera,
354 2004). For instance, absorption features (position, depth, width, and asymmetry) are used to quantitatively estimate
355 the mineral, chemical, or physiological composition of samples from the measured spectra in the field, laboratory,
356 and/or from hyperspectral images. To emphasize these absorption features, many approaches were proposed including
357 relative absorption-band-depth (Crowley et al., 1989), spectral feature fitting technique, and Tricorder and Tetracorder
358 algorithms (Clark et al., 2003). These approaches work on the so-called CRRS approach, thus recognizing that the
359 absorption in a spectrum has a continuum and individual absorption features (Clark *et al.*, 1987; Van-Der-Meera,



360 2004; Clark *et al.*, 2014). Proposed by Clark and Roush (1984), CRRS transformation and analysis allows the isolation
361 of individual absorption features in the hyperspectral signature of a specific target under investigation, analysis, and
362 comparison. It normalizes the original spectra and helps to compare individual absorption features from a common
363 baseline (Clark *et al.*, 1987). The continuum is a convex hull fit over the top of a spectrum under study using straight-
364 line segments that connect local spectra maxima. The first and last spectral data values are on the hull; therefore, the
365 first and last bands in the output continuum-removed data file are equal to 1.0. In other words, after the continuum is
366 removed, a part of the spectrum without absorption features will have a value of 1, whereas complete absorption would
367 be near to 0, and with most absorptions falling somewhere in between. The CRRS approach was used for
368 discriminating and mapping rocks mineralogy (Clark *et al.*, 1990; Clark and Swayze, 1995), land vegetation cover
369 (Kokaly *et al.*, 2003; Huang *et al.*, 2004; Manevski *et al.*, 2011), and seagrass and SAV (Barillé *et al.*, 2011; Bargain
370 *et al.*, 2012; Wicaksono *et al.*, 2019; Indayani *et al.*, 2020). In this study, the continuum algorithm implemented in the
371 ENVI image processing system was used (ENVI, 2012).

372 3.5. Spectral sampling and convolving in MSI and OLI spectral bands

373 Since 1972, the Landsat scientific collaboration program between NASA and USGS constitutes the continuous record
374 of the Earth's surface reflectivity from space. Indeed, the Landsat satellites series support five decades of a global
375 medium spatial resolution data collection, distribution, and archive of the Earth's surfaces (Bannari *et al.*, 2004;
376 Loveland and Dwyer, 2012) to support research, applications, and climate change impacts analysis at the global, the
377 regional and the local scales (Roy *et al.*, 2014 and 2016; Wulder *et al.*, 2015). Benefiting from the acquired space-
378 engineering experience, from the heritage of Landsat instruments, and the advanced development of technology during
379 the last five decades, the fourth generation of Landsat is composed of two similar sensors with very high spectral and
380 radiometric sensitivities: OLI-1 and OLI-2 (Markham *et al.*, 2016; Li and Chen, 2020). The OLI-1 carried onboard
381 Landsat-8 was launched on 11th February, 2013. While the OLI-2 will be onboard the Landsat-9 mission which is
382 currently scheduled to launch in September 2021 (NASA, 2019 and 2021). The OLI sensors collect land-surface
383 reflectivity in the VNIR, SWIR, and panchromatic wavelength with a FOV of 15° covering a swath of 185 km with
384 16 days' time repetition at the equator. The band passes are narrower to minimize atmospheric absorption features
385 (NASA, 2014), especially the NIR spectral band (0.865 μm). Two new spectral bands have been added: a deep blue
386 visible shorter wavelength (band 1: 0.433 - 0.453 μm) designed specifically for water resources and coastal zone
387 investigation and a new SWIR band (9: 1.360 - 1.390 μm) for the detection of cirrus clouds. Moreover, compared to
388 previous TM and ETM+ sensors using only 8 bit, the OLI design results in more sensitive instruments with a
389 significant improvement of the SNR radiometric performance quantized over a 12-bit dynamic range (Level 1 data),
390 and raw data are delivered in 16 bit. The high performance of SNR associated with improved radiometric and spectral
391 resolutions provide a superior dynamic range of radiance by reducing saturation problems and, therefore, enabling
392 better characterization of land and water surface conditions (Knight and Kvaran, 2014), especially with orbit reflective
393 radiometric calibration better than 3% (Markham *et al.*, 2014; Gascon *et al.*, 2017). Table 1 summarizes the effective
394 bandwidth characteristics of OLI-1 and OLI-2 sensors.

395



396 [Table 1]

397

398 Otherwise, the Sentinel-2 mission is the result of close collaboration between the European Space Agency, the
399 European Commission, industry, service providers, and data users. It is composed of two satellites, Sentinel-2A which
400 was launched in June 2015, and Sentinel-2B that was launched in March 2017. Both satellites are equipped with
401 identical MSI sensors to provide continuity to the SPOT missions and to improve the Landsat-OLI temporal frequency
402 (Drusch et al., 2012). The synergy between the four sensors (MSI-2A, MSI-2B, OLI-1, and OLI-2) significantly
403 increase the temporal resolution (around 2 days) offering new opportunities for several environmental and natural
404 resource applications, such as the vigour of vegetation cover, emergency management, water quality, seagrass
405 meadows, and climate change impacts analysis at local, regional, and global scales. The MSI images the Earth's
406 surface reflectivity with a large FOV (20.6°) in 13 spectral bands with several spatial resolutions from 10 to 60-m;
407 four bands with 10-m (blue, green, red, and NIR-1), six bands with 20-m (Red-Edge, NIR-2, and SWIR), and three
408 bands with 60-m (coastal, water vapor and cirrus). The swath of each scene is 290 km, permitting global coverage of
409 the Earth's surface every 10 days. The MSI radiometric performance is coded in 12 bits, ensuring radiometric
410 calibration accuracy of better than 3% and an excellent SNR (Markham et al., 2014; Li et al., 2017). Table 1
411 summarizes the effective bandwidth characteristics of MSI-2A and MSI-2B sensors.

412 As discussed above, the measured bidirectional reflectance factors with the ASD have a 1-nm interval allowing
413 the acquisition of 2151 contiguous hyperspectral bands per spectrum. However, most multispectral remote sensing
414 instruments measure integrated reflectance over broad bands (equation 1). Consequently, the average of 40 spectra
415 measured with the ASD over each sample was resampled and convolved to match the solar-reflective spectral
416 responses functions characterizing the optics and electronics of MSI and OLI instruments in the VNIR spectral bands
417 (Fig. 6). In this step, the resampling procedure considers the nominal width of each spectral band (Table 1). Then, the
418 convolution process was executed using the CAM5S transfer radiative code (Teillet and Santer, 1991). This
419 fundamental step simulates the signal received by the considered sensors at the top of the atmosphere from a surface
420 reflecting solar and sky irradiance at sea level, considering the filter of each band (Fig. 6), and assuming ideal
421 atmospheric conditions without scattering or absorption (Zhang and Roy, 2016). Accordingly, the equivalent
422 convolved reflectance ($\rho(\lambda_i, \lambda_s)_i$) over each sample was generated at the satellite orbit altitude in homologous VNIR
423 spectral bands of each sensor (Slater, 1980):

424

$$425 \quad \rho(\lambda_i, \lambda_s)_i = \frac{\int_{\lambda_i}^{\lambda_s} R(\lambda) S(\lambda)_i d(\lambda)}{\int_{\lambda_i}^{\lambda_s} S(\lambda)_i d(\lambda)} \quad (1)$$

426

427 Where $\rho(\lambda_i, \lambda_s)_i$ is the equivalent convolved reflectance of the band “i” of each sensor, λ_i to λ_s are the spectral
428 wavelength ranges of the band “i” of each sensor, $R(\lambda)$ is the corresponding reflectance at wavelength “ λ ” measured
429 by the ASD, and $S(\lambda)_i$ is the corresponding spectral responsivity value of the spectral response function of the band
430 “i” of each sensor (Fig. 6). It is important to note that the MSI-NIR-2 broadband (band-8: 785 - 900 nm) is not
431 considered in this study because it is not a real homologous band of OLI-NIR, and it has a greatest reflective band



432 difference with the OLI-NIR (851–879 nm). The OLI-NIR spectral response function intersects with only 20% of the
433 MSI-NIR-2 response function. Moreover, the MSI red-edge bands were not considered also as they are not acquired
434 by the OLI sensor.

435

436

[Figure 6]

437 3.6. Data Processing

438 In addition to remote sensing sensor technologies' improvement and innovation, a variety of processing methods have
439 been applied for spectral data for mapping and monitoring seagrass and habitats in shallow coastal waters. They were
440 applied to highlight the seagrass and algae species composition, leaf area index estimation, percentage cover mapping,
441 etc. They include matched filtering approach (Li et al., 2012), object-based image analysis (Roelfsema *et al.*, 2014),
442 adaptive coherence estimator and constrained energy minimization (Li et al., 2012), artificial neural network model
443 (Ressom et al., 2003; Perez et al., 2020), linear spectral mixture analysis (Uhrin and Townsend, 2016; Chen et al.,
444 2016), spectral angle mapper (Peneva et al., 2008; Li et al., 2012; Marcello et al., 2018; Wicaksono et al., 2019),
445 classification tree analysis (Wicaksono et al., 2019), random forest (Bayyana et al., 2020), support vector machines
446 (Marcello et al., 2018; Bakirman and Gumusay, 2020; Perez et al., 2020; Bayyana et al., 2020), and machine learning
447 regression (Traganos, 2020; Bakirman and Gumusay, 2020). Undeniably, these sophisticated and complicated
448 methods require extensive training information and field endmember measurements. However, the simplicity of
449 empirical and semi-empirical methods based on vegetation indices are easier to transfer between sensors and can be
450 used as a robust alternative compared to the complex processing methods; because these methods are based on the
451 knowledge of spectral absorption features that characterize specifically the target under investigation. Moreover, these
452 methods have the advantage of being reproducible, easily transferable, and applicable in other geographic regions.
453 Each method has advantages and limitations, especially in shallow water. In this study, after the spectral analysis and
454 CRRS transformation, the capability and comparison of the VNIR homologous spectral bands of MSI and OLI sensors
455 were investigated for seawater, sediments, seagrass, algae, and mixed species discrimination at different coverage
456 rates. Then, although the literature refers to more than fifty vegetation indices for land vegetation cover monitoring
457 and characterization (Bannari et al., 1995), only the most popular indices that have been used for seagrass and SAV
458 in different marine environments around the world were retained in this study. After spectral data pre-processing,
459 sampling, and convolving, the indices TGI, VARI, and Diff(G-B) were implemented and tested respecting their
460 original and unchangeable equations. While the NDVI, SAVI, EVI, TDVI, NDWI, and DVI indices were calculated
461 in three versions by integrating the red, blue, and green bands. The equations of the considered indices are as follow:

462

$$463 \text{NDVI} = (\rho_{\text{NIR}} - \rho_{\text{Red}}) / (\rho_{\text{NIR}} + \rho_{\text{Red}}) \quad (\text{Rouse et al., 1974}) \quad (2)$$

$$464 \text{SAVI} = 1.5 * (\rho_{\text{NIR}} - \rho_{\text{Red}}) / (\rho_{\text{NIR}} + \rho_{\text{Red}} + 0.5) \quad (\text{Huete, 1988}) \quad (3)$$

$$465 \text{TDVI} = 1.5 * (\rho_{\text{NIR}} - \rho_{\text{Red}}) / (\sqrt{(\rho_{\text{NIR}}^2 + \rho_{\text{Red}} + 0.5)}) \quad (\text{Bannari et al., 2002}) \quad (4)$$

$$466 \text{NDWI} = (\rho_{\text{Green}} - \rho_{\text{NIR}}) / (\rho_{\text{Green}} + \rho_{\text{NIR}}) \quad (\text{McFeeters, 1996}) \quad (5)$$

$$467 \text{EVI} = 2.5 * (\rho_{\text{NIR}} - \rho_{\text{Red}}) / (\rho_{\text{NIR}} + 6 * \rho_{\text{Red}} - 7.5 * \rho_{\text{Blue}} + 1) \quad (\text{Huete et al., 2002}) \quad (6)$$



468 $DVI = \rho_{NIR} - \rho_{Red}$ (Richardson and Wiegand, 1977) (7)

469 $VARI = (\rho_{Green} - \rho_{Red}) / (\rho_{Green} + \rho_{Red} - \rho_{Blue})$ (Gitelson et al., 2002a) (8)

470 $TGI = \rho_{Green} - 0.39 * \rho_{Red} - 0.61 * \rho_{Blue}$ (Hunt et al., 2013) (9)

471 $Diff(G-B) = \rho_{Blue} - \rho_{Green}$ (Mumby et al., 1997) (10)

472 3.7. Statistical analyses

473 As discussed previously, the MSI and OLI relative spectral response profiles characterizing the filters of each spectral
474 band are relatively different (Fig. 6). To examine the impact of this difference, statistical analyses were computed
475 using “Statistica” software. The relationships between the product values (reflectances and WVI’s) derived from MSI
476 against those obtained from OLI were analyzed between homologous bands using a linear regression model ($p < 0.05$).
477 As well, the R^2 was used to evaluate the strength of this linear relationship. For this process, the resampled and
478 convolved spectra of all samples’ reflectance data were used, and the homologous values in VNIR bands of MSI and
479 OLI were compared using the 1:1 line. Ideally, these independent variable values should have a correspondence of
480 1:1. Additionally, the root mean square difference (RMSD) between both sensors was derived (Willmott, 1982; Zhang
481 et al., 2018):

482
483
$$RMSD = \sqrt{\frac{\sum_i^n (v_i^{OLI} - v_i^{MSI})^2}{n}}$$
 (11)

484
485 Where RMSD between corresponding Landsat-OLI and Sentinel-MSI variables values (reflectances and WVI’s), “ v_i ”
486 is the variable under analysis and “ i ” is the number of variable ($i = 1$ to n).

487 4. Results analysis

488 4.1. Spectral and CRRS analysis

489 Spectral signatures of seagrass and algae species are measured separately and mixed in black and yellow large bowls
490 using two sedimentary substrates (dark and bright). They are presented separately for the examined coverage rates,
491 namely 10, 30, 75, and 100% (Fig. 7, a-d). Overall, the reflectance signatures of seagrass and algae samples are similar
492 to those of healthy vegetation canopy. These reflectance signatures exhibit slight absorption features near 450 nm and
493 others stronger between 650 and 700 nm with a minimum at 670 nm caused by the chlorophyll; as well as a significant
494 reflection between 520 and 600 nm due to carotenoid pigments and high reflectance in the NIR attributed to internal
495 tissue structure (700 to 900 nm). Differently to land vegetation, the red-edge is not well developed (very weak)
496 particularly for non-dense seagrass and algae due to high red and NIR absorption by water molecules as shown in Fig.
497 1. Generally, absorption or reflection of pigmentations between species occurs in different wavelengths but the
498 strength of absorption gradually increases in the red as the coverage rate increases.

499 For scattered and low coverage (~ 10 %), the shapes of all spectra are relatively similar, without the possibility to
500 identify specific absorption features or to separate among species according to their spectra in the visible domain (Fig.



501 7a). The highest reflectance values vary between 10% and 15% across NIR wavelengths with a difference reflectance
502 ($\Delta\rho_{\text{NIR}}$) around 5%, while in the visible all the reflectance values are below 5% with $\Delta\rho_{\text{visible}}$ are also $< 5\%$. For this
503 low and sparse cover, it is observed that the reflectance is influenced by spectral properties of the underlying
504 sediments, fragments of vegetation, light shading, etc., thus contributing to the confusion between spectral signatures.
505 Definitely, under such conditions, it is a challenge to distinguish between seagrass and/or algae species based only on
506 their spectral signatures. Whereas, the measurements acquired over somewhat denser coverage rates ($\sim 30\%$) show
507 analogous spectral behaviour and patterns with overlap among spectra in visible wavelengths (400 to 700 nm), but a
508 slight separability between species stands out relatively in NIR (Fig. 7b).

509 Furthermore, unlike scattered or less dense cover ($\leq 30\%$), the analysis of the dense and very dense coverage rates
510 (75 and 100%) showed that the optical properties (darkness or brightness) of the underlying substrate does not have a
511 significant effect on the measured spectra. For these coverage ranges, the clear and normal behaviour of vegetation
512 cover spectra are observed. The absorption feature is weak in the blue (450-480 nm) but more accentuated in red (670
513 nm), the reflection peak is more highlighted in green (550 nm), and the reflectance values increase notably and
514 gradually in NIR with the increase of the coverage rate. Although the seagrass has a distinct spectral response
515 compared to the algae, especially in the green and NIR regions of the spectrum, significant spectral differences are
516 noted for the HU with the highest reflectance, followed by GA, HS, and BA. This order is probably controlled by the
517 leaves structures that are specific for each type of seagrass or algae. The reflectance values in the visible are controlled
518 by the absorption of chlorophyll pigmentations in blue and red wavelengths, and by the carotenoid pigmentations in
519 the green band. In addition, compared to HS and BA spectra, HU and GA showed relatively strong absorption by
520 chlorophyll in red wavelengths. This difference is due to the nature of chlorophyll in each species. Indeed, brown
521 algae contain accessory pigments “fucoxanthin” and chlorophyll “c” (Johnsen and Sakshaug, 2007), while seagrass
522 are flowering plants, and their leaves contain chlorophyll “b” (Cummings and Zimmerman, 2003). It is observed also
523 that the BA carotenoid pigments (fucoxanthin) are characterized by spectral features at 630 and 650 nm that are not
524 present in the spectra of HS, HU, and GA (Fig. 7). However, despite all these spectral characteristics the difference in
525 reflectance values among all species (individual and mixed) is $\leq 6\%$ in the visible and $\leq 13\%$ in NIR for a very dense
526 cover (100%). Therefore, these results suggest that it is probably possible for the blue, green, and NIR wavelengths
527 to discriminate among the considered seagrass and algae species if they are homogeneous with high or very high
528 densities.

529 Otherwise, the CRRS transformations are presented in Fig. 7 (e-h) with Sentinel-MSI relative spectral response
530 profiles characterizing the filters of VNIR bands. The lower CRRS values indicate the greatest potential spectral
531 separability, which means the identification of the appropriate wavelengths to discriminate among the considered
532 classes of investigated species. As shown in Fig. 7 (e-h), the CRRS significantly enhances the spectral separability
533 among the seagrass and algae classes, especially in the visible bands. Two main absorption features are highlighted in
534 the blue (485-498 nm) and red (~ 670 nm) regardless the species. In the green, one major reflection peak is observed
535 around 544 nm for HU and GA, one around 530 nm for HS, and three peaks are well distinguished for BA at 578,
536 595, and 640 nm (Fig. 7h). These differentiation features become clearer as the coverage rates increase especially in
537 blue and NIR wavelengths. For a low coverage rate ($\sim 10\%$), the strongest absorption depth is that of GA (0.46)



538 followed by HU (0.58), HS (0.74), and BA (0.78) in the blue (Fig. 7e). While in the red, CRRS pointed out that
539 regardless of the coverage rate, a strong similarity is observed between HU and GA due to their
540 high content of chlorophyll pigmentation with a depth of absorption around 0.29. Subsequently
541 followed by HS and BA that are characterized by less absorption depth (~ 0.50). In these two
542 waveband domains (blue and red), the absorption features become deeper with increasing coverage density. Likewise,
543 when the cover rate of all species becomes denser (100%), similar absorption characteristics are exhibited in the red
544 band between HU and GA species; as well as between HS and BA (Fig. 7h). While in the blue and NIR wavelengths,
545 the CRRS highlights the distinction and differentiation between species. On the other hand, as the coverage increases
546 from 10 to 100%, the reflection peak in the green waveband becomes less pronounced due to the high content of
547 carotenoid pigment; also a strong similarity is observed between HU and GA. Moreover, the curves of CRRS of the
548 mixed species occupy an intermediate position of absorption features between the homogeneous samples and,
549 therefore, the differentiation between absorption characteristics becomes very narrow. Accordingly, the discrimination
550 between pure and mixed species becomes very difficult or even impossible. Overall, spectral and CRRS analyses
551 highlighted the importance of the blue, green, and NIR wavelengths for seagrass and algae detection and probable
552 discrimination based on hyperspectral measurements. These results corroborate the physical concept
553 presented in Fig. 1 that the blue and green electromagnetic radiation penetrates a deeper
554 vertical column of water. While despite its limited penetration, the NIR shows a certain
555 sensitivity to the biomass density and its spatial distribution.

556

557

[Figure 7]

558 **4.2. Resampling and convolving in OLI and MSI bands**

559 Fig. 8 illustrates the scatter-plots between the resampled and convolved reflectance values in the VNIR homologous
560 bands of the MSI and OLI sensors. Simulated at the top of the atmosphere using all considered samples (seawater,
561 sediments, seagrass, algae and mixed species of both seagrass and algae at unlike coverage rates), they allow the
562 analysis of the difference in reflectance values ($\Delta\rho$) and RMSD due exclusively to dissimilarities in spectral response
563 function between homologous bands. These scatter-plots reveal a near-perfect fit with 1:1 line expressing an excellent
564 coefficient of determination (R^2 of 0.999) between homologous bands with the slopes and intercepts very near to unity
565 and zero, respectively. Thus, the derived $\Delta\rho$ values are null for VNIR homologous bands for seawater and are
566 insignificant for dark and bright substrate sediments in all bands (i.e., 0.009 for green and 0.002 for the coastal, blue,
567 red, and NIR bands). While, for seagrass and algae (HS, HU, GA, and BA), $\Delta\rho$ vary between 0.003 and 0.02 regardless
568 of the coverage rate or the considered spectral band. Moreover, the achieved overall RMSD in reflectance between
569 MSI and OLI homologous bands considering all samples are insignificant (≤ 0.0015) for blue, green, and red bands,
570 and null for coastal and NIR bands. It is also observed that all the bands are insensitive to the variation of the colors
571 of the bowls and the sedimentary substrate optical properties. These results pointed out that MSI and OLI sensors are
572 spectrally similar and can be used jointly for high temporal frequency to monitor seagrass and algae dynamics in time



573 and space. Therefore, due to this near-perfect spectral similarity between these instruments, our analysis in the
574 following sections will focus only on the MSI sensor.

575

576 [Figure 8]

577

578 Fig. 9 illustrates the reflectances of seagrass, algae, and seawater resampled and convolved in VNIR bands of MSI or
579 OLI sensors considering each species separately and all species at different coverage rates. Compared to the measured
580 hyperspectral signatures (Fig. 7), these broadband spectra are more generalized and less precise because these spectra
581 lost the specific and unique absorption features of seagrass and/or algae species caused by pigmentations as discussed
582 above. However, such broadband spectra still retain the same spectral pattern as the original spectra. Regardless of
583 the species, the graphics summarized in Fig. 9 exhibit similar shape and pattern, but with a slight difference in
584 reflectance values between species in the visible bands. If we consider the species separately (HS, HU, GA, and BA)
585 in different coverage rates (10, 25, 75, and 100%), the reflectance difference values ($\Delta\rho$) are ≤ 0.02 ; and insignificant
586 ($\Delta\rho \leq 0.002$) for pure seawater and sediments in all VNIR bands. Hence, these species are not spectrally
587 distinguishable particularly in the visible whatever the coverage. While, if we consider all samples (seagrass, algae,
588 and mixed) in all coverage rates (Fig. 9e), the $\Delta\rho$ are equal to 0.03 in coastal and blue bands, 0.05 in green, 0.035 in
589 red and 0.21 in NIR. Except for the NIR, the calculated $\Delta\rho$ values in the visible are approximately identical to the
590 accuracies achieved from radiometric calibration and atmospheric corrections. Therefore, relying on the multispectral
591 bandwidth of OLI and MSI sensors, it is difficult or even impossible to differentiate or to map seagrass and algae
592 individually at the species level. Accordingly, SAV classes' discrimination and mapping will be discussed.

593

594 [Figure 9]

595 4.3. Vegetation indices analysis

596 In this third part, the NDVI, SAVI, EVI, TDVI, NDWI, and DVI indices were implemented and analysed in three
597 versions each by integrating the red, blue, and green bands; while the indices TGI, VARI, and Diff(G-B) were
598 calculated and tested respecting their original and unchangeable equations. In total, 21 combinations of indices were
599 calculated for each sensor. The statistical analyses ($p < 0.05$) focus on the similarity or dissimilarity between MSI and
600 OLI homologous indices, and their potential for seagrass and algae discrimination. Except for the TGI and VARI
601 indices, the results revealed an excellent linear relationship (R^2 of 0.999) between MSI and OLI products regardless
602 of the compared index and the integrated spectral bands (red, green, and blue). Overall, the scatter-plots presented in
603 Fig. 10 depict a very good fit to the 1:1 line with the slopes and intercepts very near to unity and zero, respectively.
604 However, despite its near-perfect linearity and insignificant RMSD between MSI and OLI values (0.001), the TGI
605 show a very weak and limited spatial variability with a range between 0 for pure seawater and 0.05 for a very dense
606 coverage (100%) of seagrass or algae (Fig. 10e). This range cannot allow the differentiation among the marine
607 environment classes, because this index was not developed for biomass sensing but was designed for crop nitrogen
608 requirements detection. Likewise, although the scatter-plot of VARI shows an excellent coefficient of determination



609 (R^2 of 0.99), this index overestimates the predicted values by MSI sensor compared to those estimated by OLI,
610 resulting in the data not fitting the 1:1 line very well (Fig. 10f). Moreover, the difference
611 values of VARI derived from MSI and OLI data vary between 0 and 0.14 depending on the sample species and its
612 coverage rate, with an overall RMSD of 0.03. This result can be explained by the fact that the VARI uses only the
613 visible ranges of the spectrum and does not consider the NIR band which is the most informative about the biomass
614 density. In addition, it was developed particularly for very dense (100%) wheat crops; moreover, it was designed
615 principally for coarse data acquired by the SeaWiFS, MODIS, MISR, and MERIS sensors. According to Gitelson et
616 al. (2002b), many factors potentially decrease the accuracy of the VARI such as vegetation cover species, canopy
617 architecture, and sun illumination geometry. For wheat and corn species, this index yielded RMSE of around 10%
618 (Gitelson et al., 2002a). Therefore, the weaknesses raised for these two indices (TGI and VARI) are not caused by the
619 impact due exclusively to the dissimilarities in spectral response function between homologous bands of MSI and OLI
620 sensors, but due to their mathematical concepts that are intended for a single and specific application.

621 Furthermore, the scatter-plots presented in Fig. 10 (a-d) are showing examples of certain indices including
622 NDWI, WAVI, WEVI, and WTDVI. Overall, the indices are fitting very well the 1:1 line with R^2 of 0.99, slopes very
623 near to unity and intercepts to zero. The indices show that the derived WVI from MSI and OLI data are predicting
624 similarly seagrass and algae species in a shallow marine environment. Considering all investigated samples in this
625 study, the interval difference values between homologous indices vary between 0 and 0.01 for all versions of WTDVI,
626 WAVI, WDVI, and Diff(G-B); while they vary between 0 and 0.04 for NDWI, WEVI and NDWI. These differences
627 values are satisfactory and remain equal or less than the combined inaccuracies of atmospheric corrections and sensor
628 radiometric calibration. Moreover, the achieved RMSD values between MSI and OLI homologous indices are
629 insignificant ($RMSD \leq 0.01$) for all indices (Table 2) regardless of the integrated spectral band. These analyses pointed
630 out that MSI and OLI sensors can be combined for high temporal frequency to monitor the dynamic of biophysical
631 products in time and space in a shallow marine environment.

632

633 [Table 2]

634

635 [Figure 10]

636

637 Fig. 11 summarises the linear regressions ($p < 0.05$) between the best indices and the reflectances in NIR considering
638 all samples, i.e., seawater, sediments, seagrass, algae, and mixed species classes with different coverage rates (10, 30,
639 75, and 100%). The computed indices (NDVI, SAVI, EVI, TDVI, NDWI, and DVI) with the blue, green, and red
640 bands are the most relevant for SAV differentiation and mapping. Firstly, it is observed that the indices NDVI and
641 NDWI provided similar results with opposite signs, i.e., symmetrically opposed concerning the X-axis. Indeed,
642 whatever the integrated band, the NDWI results are always symmetrical compared to those of NDVI but with negative
643 values. However, such results are not showing the truth because negative values are automatically reset to zero by the
644 image processing system and, therefore, it is probable that the results will be inaccurate. Furthermore, when the red
645 and blue bands are implemented in the NDVI equation, insignificant fits (R^2 of 0.40) were achieved; but improved



646 results are obtained with the integration of the green band (R^2 of 0.63) and the index is named NDWVI. Analogous
647 results are obtained by Diff(G-B) and VARI indices with R^2 of 0.63 (Table 2) when all samples are considered.
648 Luckily, the statistical fits of these three indices (NDWVI, Diff(G-B), and VARI) becomes significantly improved
649 when unique species is considered, such as only seagrass or only algae (R^2 of 0.85). Whereas, in addition to its
650 weakness and limited sensitivity to the spatial variability of seagrass and algae, the TGI was irrelevant for SAV
651 discrimination yielding a very low fits (R^2 of 0.20) whatever the considered species.

652

653 [Figure 11]

654

655 As discussed previously, when integrating the blue and green bands, the indices WdVI, WdVI, WEVI, and
656 WTDVI outperformed all examined indices regardless of the species (seagrass, algae, or mixed), yielding a very
657 significant coefficient of determination for mixed species ($0.89 \leq R^2 \leq 0.96$) (Fig. 11 a-d, and Table 2). Calculated
658 with blue, green, or red bands, the DVI (noted WdVI) discriminated among SAV classes significantly ($R^2 \leq 0.92$),
659 but it underestimates the SAV as shown in Fig. 10-d. However, WdVI, WEVI, and WTDVI offer similar trends
660 regardless the considered species ($R^2 \leq 0.92$ for mixed or seagrass only, and R^2 of 0.82 for algae only). Overall, instead
661 of the red band, the integration of blue and green bands in vegetation indices increases their discriminating power for
662 SAV (Table 2). These results corroborate the spectral analysis and the CRRS transformations; the blue and green
663 electromagnetic radiation penetrates deeper through the water allowing more details and information about marine
664 vegetation discrimination. This finding is consistent with Wicaksono and Hafizt (2013), and Villa et al. (2014) where
665 the blue band better separates and maps aquatic vegetation features over some lake ecosystems in Italy. However, the
666 summarized R^2 in Table 2 shows that the indices WdVI, WEVI, and WTDVI provided relatively identical results
667 when integrating the blue or green bands. Nevertheless, the scatter plots in Fig. 11 (a, b, and c) illustrate that when the
668 green band is considered instead of the blue, the majority of sampled points are located closer to line 1:1, especially
669 when the coverage rate becomes denser. This can be explained by the fact that despite the power of blue wavelengths
670 to penetrate deeper into the water, this band also leads to an overestimation of indices values due to its higher scattering
671 (Fig. 11), mainly in turbid environments.

672 5. Discussion

673 Seagrass and algae species showed similar spectral signature curves, but with subtle differences between species. In
674 general, some relevant wavelengths are observed for the characterization of the considered species of seagrass and
675 algae including those at or near 450, 500, 520, 550, 600, 620, 640, 670, and 700 nm. They are related to the absorption
676 features and reflection peaks due to photosynthetic pigmentations of HU, HS, GA, and BA. Spectral and CRRS
677 analyses highlighted the importance of the blue, green, and NIR wavelengths for probable differentiation between the
678 considered seagrass and algae types. However, the magnitude of the $\Delta\rho$ values among species is an indicator of the
679 strength of the absorption feature depths and, therefore, of their discriminating power between species. For instance,
680 the highest $\Delta\rho$ values among all considered samples (seagrass, algae, and mixed of both) is $\leq 5\%$ across the visible
681 wavelengths and around 10 to 15% in NIR. Likewise, the CRRS transformations of all spectra of homogeneous and



682 mixed samples show that the absorption characteristics become very narrow and, thus, the discrimination between
683 pure and mixed species becomes difficult or even impossible. These results are in agreement with other findings that
684 have been conducted in many geographic locations worldwide and have considered many seagrass and algae types.
685 Considering nine tropical species of seagrass, Wicaksono et al. (2019) showed that even hyperspectral data will not
686 improve discrimination between seagrass and algae at the species level in pixels or sub-pixels due to the subtle
687 difference in absorption features among them. As well, Phinn *et al.* (2008) confirmed that the hyperspectral data are
688 unable to map seagrass biomass at the species level in shallow waters of Moreton Bay in Australia. Using field and
689 laboratory hyperspectral measurements over several seagrass species on the west coast of Florida, Pu et al. (2012)
690 reported also that the VNIR wavelengths have relatively low accuracies to discriminate among seagrass community
691 composition.

692 Otherwise, the resampled and convolved spectra in VNIR bands of MSI and OLI sensors are similar in all cases,
693 considering each species separately or the totality of samples at different coverage rates. These spectra are more
694 generalized and less precise due to the loss of absorption features caused by pigmentations. Hence, regardless of the
695 coverage rates, if the pure and homogenize species are considered, the $\Delta\rho$ is ≤ 0.02 in the visible and is ≤ 0.22 in NIR.
696 While, if all mixed samples and species are considered at the investigated coverage rates, $\Delta\rho$ is ≤ 0.05 in visible bands
697 and remains stable ($\Delta\rho \leq 0.22$) in NIR. These very narrow values do not allow spectral distinction among species,
698 particularly in the visible wavebands. Therefore, relying on the multispectral bandwidth of OLI and MSI sensors, it is
699 difficult to differentiate seagrass and algae individually at the species level. Indeed, it is important to remember that
700 these simulations were conducted in a Goniometric-Laboratory using close range measurements protocol and
701 supervising rigorously all measured samples, i.e., homogeneous, or mixed. Moreover, in this controlled environment,
702 the atmospheric scattering and absorption are absent; errors related to the sensor radiometric calibration are also
703 absent, no wave's variation, no residual clouds contamination, no sun-glint (specular effects), no variability in water
704 depth, and no BRDF impact. However, the results obtained are not entirely conclusive and do not provide a clear and
705 satisfactory distinction among the spectral signatures of the investigated species. The difference among spectral
706 signatures is surely reduced in the real world when seagrasses and algae are embedded in sediments and overlaid by
707 water column and constituents including phytoplankton, suspended organic and inorganic matter, variability in water
708 depth, and remote sensing problems (internal and external). Additionally, the acquired images with Sentinel-MSI (2A
709 and 2B) and Landsat-OLI (8 and 9) sensors are coded radiometrically in 12 and 16 bits, respectively. These images
710 cover dissimilar pixels surfaces of 100 m² for MSI and 900 m² for OLI, where SAV information can be easily mixed
711 within pixels. Besides, the FOV of these instruments are different, OLI's FOV is 15° covering a swath of 185 km,
712 while the MSI is characterized by a large FOV of 20.6° covering a swath of 290 km, which requires the adjustments
713 to reduce differences caused by BRDF effects (acquisition and sun illumination geometries). Data quality may also
714 change due to the sensor's radiometric performance, SNR, and atmospheric interferences (diffusion and absorption).
715 Nevertheless, despite the corrections of all these anomalies before the information extraction, biases still occur
716 generated by errors propagation, which affect the recorded signal at the sensor level and, therefore, the precision of
717 discrimination between seagrass and algae at the species level. For instance, if we consider the published RMSE
718 regarding each source of error separately, the calculated total RMSE based on errors propagation theory (equation 12)



719 will be approximately 0.08 to 0.10 (reflectance unit). Therefore, this total RMSE is greater than the achieved difference
720 between reflectance values ($\Delta\rho \leq 0.05$), especially in the visible bands. Accordingly, it is impossible to differentiate
721 between seagrass and algae at the species level. Likewise, this total RMSE is solely due to the limitations
722 of remote sensing methods, but it can also be amplified by environmental restrictions of
723 seagrass habitat, as discussed above and reported by Wicaksono and Hafizt (2013).

724

$$725 \text{RMSE-Total} = [(\sigma\text{-Sensor-drift})^2 + (\sigma\text{-Atmosphere})^2 + (\sigma\text{-Sun-glnt})^2 + (\sigma\text{-BRDF})^2 + (\sigma\text{-Water-column})^2]^{0.5} \quad (12)$$

726

727 Where:

728 $\sigma\text{-Sensor-drift}$: Sensor radiometric calibration accuracy, ± 0.03 (Markhman et al., 2014 and 2016),

729 $\sigma\text{-Atmosphere}$: Atmospheric corrections accuracy, mostly around ± 0.03 to ± 0.05 in the visible bands
730 (Vermote et al., 2016),

731 $\sigma\text{-Sun-glnt}$: Sun glint correction accuracy, ± 0.05 (Zorrilla et al., 2019),

732 $\sigma\text{-BRDF}$: Accuracy of BRDF correction for MSI, ± 0.05 to ± 0.08 (Roy et al., 2017),

733 $\sigma\text{-Water-column}$: Accuracy of water column correction, ± 0.04 (Zoffoli et al., 2014).

734

735 The results of this research accomplished in the Arabian Gulf species based on spectroradiometric measurements are
736 consistent with other researches carried out in many geographical regions worldwide. Barillé et al. (2009) showed the
737 degradation of spectral features when resampled into SPOT-HRV visible bands and, therefore, seagrass species could
738 no longer be discriminated in these wavelengths. This statement is also in agreement with Wicaksono et al. (2017)
739 who reported that resampled spectra in MSI and OLI bands do not have sufficient spectral information for seagrass
740 species discrimination for accurate classification. Moreover, it was reported that sub-pixel species composition and
741 mixing added complexity to seagrass species mapping even using hyperspectral data and advanced image processing
742 approaches (Phinn et al., 2008; Joyce et al., 2013; Hedley et al., 2012a and 2012b). For instance, Wicaksono et al.
743 (2019) highlighted the limitation of SAM for seagrass mapping due to the similarity of absorption features among the
744 spectral signatures of the mapped seagrass species. As well, Chen et al. (2016) revealed the difficulty and limitation
745 of LSMA for mapping scattered and heterogeneous seagrass patches that are smaller than the pixel size due to spectral
746 confusion between the seagrass and other SAV classes. Using MSI and OLI data with respectively 10 m and 30 m
747 pixel sizes (i.e., each OLI pixel is represented by 9 MSI pixels), Lyons et al. (2011) reported relatively accurate
748 discrimination between seagrass meadows spots that are very large with homogenous composition and distinct
749 boundaries between species. However, if the analyzed patches are heterogeneous, composed of diverse species and
750 scattered without clear boundary, then the differentiation becomes impossible. Therefore, SAV classes' discrimination
751 and mapping need to be thoroughly adopted to be able to map seagrass and algae on species level rather than relying
752 on the multispectral bandwidth of OLI and MSI sensors.

753 Furthermore, to analyze the impact of differences in reflectance exclusively due to dissimilarities in spectral
754 response function between homologous spectral bands, the scatter-plots between SMI and OLI simulated surface



755 reflectance values at the top of the atmosphere revealed a very good linear relationship (R^2 of 0.999) between VNIR
756 homologous bands. The slopes and intercepts are nearly equal to unity and zero, respectively. It is also observed that
757 independently to the sediments substrate (dark and bright) or the color of used bowls (black or yellow), the $\Delta\rho$ values
758 between VNIR homologous bands vary in the range of 0.003 to 0.02, regardless of the observed species (seagrass,
759 algae and mixed) or the coverage rate. Moreover, the achieved overall RMSD in reflectance values are very small (\leq
760 0.0015) for all VNIR bands, i.e., smaller than the uncertainty of the radiometric calibration process (0.03) as
761 demonstrated by Markham et al. (2016). In other respect, all the derived homologous WVI values fit near-perfectly
762 with the 1:1 line expressing an excellent coefficient of determination (R^2 of 0.99), a slope of 0.99 and intercept equal
763 to zero. Moreover, the achieved RMSD values between MSI and OLI homologous indices are insignificant ($\text{RMSD} \leq$
764 0.01) for all indices regardless of the integrated spectral band (red, green, and blue).

765 These results corroborate the finding of Wicaksono et al. (2019) who reported that MSI and OLI had similar results
766 for tropical seagrass species analysis using simulated reflectance spectra and imagery data. Moreover, using simulated
767 data and real images acquired simultaneously with MSI and OLI over a wide variety of land cover types including
768 open shallow water, Mandanici and Bitelli (2016) showed a very high coefficient of determination (R^2 of 0.98)
769 between homologous bands. Comparing surface reflectances and derived biophysical variables over Australian
770 territory, Flood (2017) indicated good compatibility between SMI and OLI instruments with an $\text{RMSD} < 0.03$ for
771 surface reflectance in VNIR bands, and an RMSD around 0.05 for biophysical variables. Pastick et al. (2018)
772 demonstrated that observations made by MSI, and OLI can be used to monitor vegetation phenology accurately in dry
773 lands of the Western United States. In Europe, the comparison of surface reflectances and biophysical products of
774 various natural test sites showed a good relationship between MSI and OLI products, yielding RMSD values around
775 0.03 reflectance units (Vuolo et al., 2016). Excellent consistency and similarity have also been demonstrated between
776 these sensors for soil observation and modeling in the Middle East (Bahrain) and North Carolina in the USA (Bannari
777 et al., 2020; Davis et al., 2019). Therefore, these results pointed out that the examined sensors, MSI onboard Sentinel-
778 2A/2B and OLI onboard Landsat-8/9, can be combined for the marine environment and SAV detection, mapping, and
779 monitoring during shorter time intervals or for consecutive observations. However, rigorous pre-processing issues
780 (sensors calibration, atmospheric corrections, sun-glint corrections, and BRDF normalization) must be addressed
781 before the joint use of acquired data with these sensors. Furthermore, we demonstrated that blue and green bands are
782 better than red for seagrass and algae biomass discrimination, providing the best R^2 and the most insignificant RMSD
783 for the investigated indices. Nevertheless, it is preferable to consider the green band integration due to its sensitivity
784 to pigment content within seagrass and algae tissues, for its ability to penetrate water, and for its low sensibility to
785 atmosphere and water column scattering compared to the blue band.

786 6. Conclusions

787 The MSI sensors onboard Sentinel satellites 2A/2B and the OLI instruments installed on Landsat 8/9 satellites are
788 designed to be similar in the perspective that their data be used together to support global Earth surface reflectances
789 coverage for science and development applications at medium spatial resolution and near-daily temporal resolution.
790 However, relative spectral response profiles characterizing the filter's responsivities of these instruments are not



791 identical between the homologous bands, so some differences are probably expected in the recorded shallow water
792 reflectance values for seagrass, algae, and mixed species differentiation and mapping. Based on spectral analysis and
793 CRRS transformation, the results of the present research pointed out subtle spectral differences between seagrass (HU
794 and HS), algae (green and brown), or mixed species, particularly in the blue, green, and NIR wavelengths. However,
795 once resampled and convolved in MSI and OLI homologous VNIR bands, similar patterns to the original spectra are
796 observed but with severe generalisation and loss of specific absorption features. Therefore, mapping seagrass and/or
797 algae at the species level in shallow marine waters is a very difficult if not impossible task, either using multispectral
798 bandwidth of MSI and OLI sensors or even hyperspectral data. Moreover, different from these ideal simulations in a
799 controlled environment, the mapping would be more difficult in a real marine habitat where various
800 species are mixed and interleaved with each other, as well as the propagation of internal and
801 external errors related to remote sensing data. Hence, it is recommended to discuss SAV rather
802 than the mapping seagrass or algae at the species level. Moreover, instead of the red band, the
803 integration of the blue and green bands in WVI increases their discriminating power and ability of map SAV,
804 particularly WAVI, WEVI, and WTDVI indices. These results corroborate the spectral analysis and the CRRS
805 transformations that the blue and green electromagnetic radiation allows better marine vegetation
806 differentiation. Nevertheless, despite the power of blue wavelength to penetrate deeper into the water, it also
807 leads to a relative overestimation of dense SAV coverage due to the higher scattering in this part of the spectrum,
808 particularly in the turbid environment. Furthermore, statistical fits between SMI and OLI simulated surface
809 reflectance over the considered samples reveal an excellent linear relationship (R^2 of 0.999) between all homologous
810 VNIR bands. The achieved RMSD values are extremely small between the NIR homologous bands and insignificant
811 for the other bands (≤ 0.0015). Moreover, independently of the analysed samples, homogeneous (seagrass or algae)
812 or mixed (seagrass plus algae), good agreements ($0.63 \leq R^2 \leq 0.96$) were also obtained between homologous WVI
813 regardless of the integrated spectral bands (i.e., red, green, and blue), yielding insignificant RMSD (≤ 0.01). These
814 achieved RMSD values for reflectances or WVI's are less than the combined errors related to sensor radiometric
815 calibration and atmospheric corrections. Accordingly, these results pointed out that MSI and OLI sensors are spectrally
816 similar and can be combined for high temporal frequency to monitor accurately the SAV and its dynamic in time and
817 space in the shallow marine environment. However, rigorous pre-processing issues such as sensors calibration,
818 atmospheric corrections, BRDF normalisation, sun glint, and water column corrections must be addressed before the
819 joint use of acquired data with these sensors.

820

821 **7. Author Contributions:** Professor A. Bannari performed the paper conceptualization, field data collection, pre-
822 processing and processing, results analyses and paper writing. Professor S.T. Ali assisted in the field sampling, the
823 results analyses and the paper writing. Professor A. Abuhussain assisted in the results interpretation, analyses and
824 paper writing. All authors have read and agreed to the published version of the manuscript.

825

826 **8. Competing Interests:** The authors declare no conflict of interest.

827



828 **9. Acknowledgements**

829 The authors would like to thank the Arabian Gulf University (Kingdom of Bahrain) for the financial support for the
830 field data collection, and to Marine and Environment Arabia Consultancy Services (Manama, Bahrain), for providing
831 photographs and making them available for consultation and public use. Our gratitude goes also to the anonymous
832 reviewers for their constructive comments.

833

834 **10. References**

835 Ackleson, S. G. and Klemas, V.: Remote sensing of submerged aquatic vegetation in lower Chesapeake Bay: A
836 comparison of Landsat MSS to TM imagery. *Remote Sensing of Environment*, 22(2), 235–248, 1987.

837 Anders, K. and Lina, N.: Remote sensing of seagrasses in a patchy multi-species environment. *International Journal*
838 *of Remote Sensing*, 32(8), 2227 – 2244, 2011.

839 ASD: Analytical Spectral Devices. Technical Guide, 4th ed.; ASD Inc.: Boulder, CO, USA. Available online:
840 <http://www.asdi.com/products-spectroradiometers.asp> (accessed on 30 September 2020), 2015.

841 Bakirman, T. and Gumusay, M. U.: Assessment of Machine Learning Methods for Seagrass Classification in the
842 Mediterranean. *Baltic J. Modern Computing*, 8(2), 315-326. <https://doi.org/10.22364/bjmc.2020.8.2.07> , 2020.

843 Bannari, A.: Synergy between Sentinel-MSI and Landsat-OLI to Support High Temporal Frequency for Soil Salinity
844 Monitoring in an Arid Landscape. In: *Research Developments in Saline Agriculture*, edited by Jagdish Chander
845 Dagar, Rajender Kumar Yadav, and Parbodh Chander Sharma. Published by Springer Nature Singapore Pte Ltd.,
846 pp. 67-93, ISBN: 978-981-13-5831-9. https://doi.org/10.1007/978-981-13-5832-6_3, 2019.

847 Bannari, A., Morin, D., Huete, A. R. and Bonn, F.: A Review of Vegetation indices. *Remote Sensing Reviews*, 13,
848 95-120, 1995.

849 Bannari, A., Asalhi, H. and Teillet, P. M.: Transformed Difference Vegetation Index (TDVI) for Vegetation cover
850 Mapping. *International Geoscience and Remote Sensing Symposium (IGARSS'2002)*, Toronto, Ontario, 9-13
851 July, pp. 3053-3055, 2002.

852 Bannari, A., Teillet, P. M., and Landry, R.: Comparaison des réflectances des surfaces naturelles dans les bandes
853 spectrales homologues des capteurs TM de Landsat-5 et TME+ de Landsat-7. *Revue Télédétection*, 4(3), 263-275,
854 2004.

855 Bannari, A. and Kadhém, G.: MBES-CARIS Data Validation for Bathymetric Mapping of Shallow Water in the
856 Kingdom of Bahrain on the Arabian Gulf. *Remote Sensing*, 9, 385-404, 2017.

857 Bannari, A. and Al-Ali, Z.: Ground Reflectance Factor Retrieval from Landsat (MSS, TM, ETM+, and OLI) Time
858 Series Data based on Semi-empirical Line Approach and Pseudo-invariant Targets in Arid Landscape.
859 *International Geoscience and Remote Sensing Symposium (IGARSS-2020)*, July 19-24th, Waikoloa, Hawaii,
860 USA, pp. 5990-5993, 2020.

861 Bannari, A., Hameid, N. Abuelgasim, A. and El-Battay, A.: Sentinel-MSI and Landsat-OLI Data Quality
862 Characterization for High Temporal Frequency Monitoring of Soil Salinity Dynamic in an Arid Landscape. *IEEE*
863 *Journal of Selected Topics in Applied Earth Observations and Remote Sensing (J-STARS)*, 13(1), 2434-2450,
864 2020.



- 865 Barillé, L., Mouget, J. L., Méléder, V., Rosa, P., Jesus, B.: Spectral response of benthic diatoms with different
866 sediment backgrounds. *Remote Sensing of Environment*, 115(4), 1034–1042, 2011.
- 867 Barillé, L., Robin, M., Harin, N., Bargain, A. and Launeau, P.: Increase in seagrass distribution at Bourgneuf Bay
868 (France) detected by spatial remote sensing. *Aquatic Botany*, 92(3), 185–194, 2010.
- 869 Bargain, A., Robin, M., Le-Men, E., Huete, A. R. and Barillé, L.: Spectral response of the seagrass *Zostera noltii* with
870 different sediment backgrounds. *Aquatic Botany*, 98, 45–56, 2012.
- 871 Bayyana, S., Pawar, S., Gole, S., Dudhat, S., Pande, A., Mitra, D., Johnson, J. A. and Sivakumar, K.: Detection and
872 mapping of seagrass meadows at Ritchie’s archipelago using Sentinel 2A satellite imagery. *Current Science*,
873 118(8), 1275–1282. DOI: 10.18520/cs/v118/i8/1275-1282, 2020.
- 874 Ben-Dor, E., Ong, C. and Lau, I. C.: Reflectance measurements of soils in the laboratory: Standards and protocols.
875 *Geoderma*, 245–246, 112–124, 2015.
- 876 Boström, C., Pittman, S., Kneib, R. and Simenstad, C.: Seascape ecology of coastal biogenic habitats: advances, gaps
877 and challenges. *Marine Ecology Progress Series*, 427, 191–217, 2011.
- 878 Burfeind, D. D. and Stunz, G. W.: The effects of boat propeller scarring intensity on nekton abundance in subtropical
879 seagrass meadows. *Marine Biology (Berlin)*, 148, 953–962, 2006.
- 880 Candra, E. D., Hartono, and Wicaksono, P.: Above Ground Carbon Stock Estimates of Mangrove Forest Using
881 Worldview-2 Imagery in Teluk Benoa, Bali. *IOP Conference Series: Earth and Environmental Science*, 47(1).
882 <https://doi.org/10.1088/1755-1315/47/1/012014>, 2016.
- 883 Chen, C.-F., Lau, A.-K., Chang, N.-B., Son, N.-T., Tong, P.-H.-S and Chiang, S.-H.: Multi-temporal change detection
884 of seagrass beds using integrated Landsat TM/ETM+/OLI imageries in Cam Ranh Bay, Vietnam. *Ecological*
885 *Informatics*, 35, 43–54, 2016.
- 886 Clark, R. N. and Roush, T. L.: Reflectance spectroscopy: Quantitative analysis techniques for remote sensing
887 applications. *Journal of Geophysical Research*, 89, 6329–6340, 1984.
- 888 Clark, R. N., King, T. V. V. and Gorelick, N. S.: Automatic continuum analysis of reflectance spectra. In *JPL*
889 *Proceedings of the 3rd Airborne Imaging Spectrometer Data Analysis Workshop*, 138–142. Available on line:
890 <https://ntrs.nasa.gov/archive/nasa/casi.ntrs.nasa.gov/19880004388.pdf> (accessed on 18 March 2021), 1987.
- 891 Clark, R. N., Gallagher, A. J. and Swayze, G. A.: Material absorption-band depth mapping of imaging spectrometer
892 data using the complete band shape least-squares algorithm simultaneously fit to multiple spectral features from
893 multiple materials. In: *Proceedings of the Third Airborne Visible/Infrared Imaging Spectrometer (AVIRIS)*
894 *Workshop*, NASA - Jet Propulsion Laboratory Publications, No. 90-54, pp. 176–186, 1990.
- 895 Clark, R. N. and Swayze, G. A.: Mapping minerals, amorphous materials, environmental materials, vegetation, water,
896 ice and snow, and other materials. The USGS Tricorder algorithm, in Green, R.O., ed., *Summaries of the fifth*
897 *annual NASA Jet Propulsion Laboratory airborne earth science workshop: Pasadena*, NASA Jet Propulsion
898 *Laboratory Publication*, 95(1), 39–40, 1995.
- 899 Clark, R. N., Swayze, G. A., Carlson, R., Grundy, W. and Noll, K.: Spectroscopy from Space. *Reviews in Mineralogy*
900 *and Geochemistry*, 78(1), 399–446. DOI:10.2138/rmg.2014.78.10, 2014.



- 901 Crowley, J. K., Brickey, D. W. and Rowan, L. C.: Airborne imaging spectrometer data of the Ruby Mountains,
902 Montana: mineral discrimination using relative absorption band-depth images. *Remote Sensing of Environment*,
903 29(2), 121–134. [https://doi.org/10.1016/0034-4257\(89\)90021-7](https://doi.org/10.1016/0034-4257(89)90021-7), 1989.
- 904 Cummings, M. E. and Zimmerman, R. C.: Light harvesting and the package effect in the seagrasses *Thalassia*
905 *testudinum* Banks ex König and *Zostera marina* L.: Optical constraints on photo-acclimation. *Aquatic Botany*, 75,
906 261–274, 2003.
- 907 Dahdouh-Guebas, F., Coppejans, E. and Van-Speybroeck, D.: Remote sensing and zonation of seagrasses and algae
908 along the Kenyan coast. *Hydrobiologia*, 400, 63–73, 1999.
- 909 Dattola, L., Rende, S. F., Dominici, R., Lanera, P., Di-Mento, R., Scalise, S., Cappa, P., Oranges, T. and Aramini, G.:
910 Comparison of Sentinel-2 and Landsat-8 OLI satellite images vs. high spatial resolution images (MIVIS and
911 WorldView-2) for mapping *Posidonia oceanica* meadows. Proceedings of SPIE 10784, Remote Sensing of the
912 Ocean, Sea Ice, Coastal Waters, and Large Water Regions, 10 October 2018, Vol. 10784, 1078419-1; doi:
913 10.1117/12.2326798, 2018.
- 914 Davis, E., Wang, C. and Dow, K.: Comparing Sentinel-2 MSI and Landsat 8 OLI in soil salinity detection: a case
915 study of agricultural lands in coastal North Carolina”. *Int. J. of Remote Sens.*, 40(16), 6134–6153. DOI:
916 10.1080/01431161.2019.1587205, 2019.
- 917 Davranche, A., Lefebvre, G. and Poulin, B.: Wetland monitoring using classification trees and SPOT-5 seasonal time
918 series. *Remote Sensing of Environment*, 114(3), 552–562, 2010.
- 919 Dean, A. and Salim, A.: Remote sensing for the sustainable development of offshore mariculture. In: *A global*
920 *assessment of offshore mariculture potential from a spatial perspective*, edited by: Kapetsky, J. M., Aguilar-
921 Manjarrez, J. and Jenness, J.: FAO Fisheries and Aquaculture Technical Paper N. 549, Rome, Italy, 181 pp, 2013.
- 922 Dekker, A. G., Hestir, E. L., Malthus, T. J. and Thankappan, M.: Continental Scale Aquatic Habitat Monitoring Using
923 Sentinel-2. ESA-ESRIN, Frascati, Italy, 23 to 27 April; 28 pp, 2012
- 924 Den-Hartog, C.: *The seagrasses of the world*. North-Holland Publishing Company, Amsterdam, Netherland, 275 pp.
925 <https://doi.org/10.1002/iroh.19710560139>, 1970.
- 926 Dierssen, H. M., Chlus, A. and Russell, B.: Hyperspectral discrimination of floating mats of seagrass wrack and the
927 macroalgae *Sargassum* in coastal waters of Greater Florida Bay using airborne remote sensing. *Remote Sensing*
928 *of Environment*, 167, 247–258, 2015.
- 929 Drusch, M., Del-Bello, U., Carlier, S., Colin, O., Fernandez, V., Gascon, F., Hoersch, B., Isola, C. Laberinti, P.,
930 Martimort, P., Meygret, A., Spoto, F., Sy, O., Marchese, F., Bargellini, P.: Sentinel-2: ESA’s optical high-
931 resolution mission for GMES operational services. *Remote Sensing of Environment*, 120, 25–36.
932 <https://doi.org/10.1016/j.rse.2011.11.026>, 2012.
- 933 Duarte, C. M. and Gattuso, J.-P.: Seagrass meadows. In *Encyclopedia of Earth*. Edited by Cutler J. Cleveland;
934 Environmental information coalition National Council for Science and the Environment, Washington, DC, USA,
935 2008.
- 936 Duarte, C. M., Losada, I. J., Hendriks, I. E., Mazarrasa, I. and Marbà, N.: The role of coastal plant communities for
937 climate change mitigation and adaptation. *Nature Climate Change*, 3(11), 961–968.



- 938 <https://doi.org/10.1038/nclimate1970>, 2013.
- 939 Duffy, J. P., Pratt, L., Anderson, K., Land, P. E. and Shutler, J. D.: Spatial assessment of intertidal seagrass meadows
940 using optical imaging systems and a lightweight drone. *Estuarine, Coastal and Shelf Science*, 200, 169–180, 2018.
- 941 Dunton, K. H., and Schonberg, S. V.: Assessment of propeller scarring in seagrass beds of the south Texas coast:
942 *Journal Coastal Research*, 37, 100–110, 2002.
- 943 ENVI: Continuum Removal Tutorial. Boulder, Colorado, USA.
944 <http://www.harrisgeospatial.com/docs/ContinuumRemoval.html> , 2017.
- 945 Erfteimeijer, P. L. A. and Shuail, D. A.: Seagrass Habitats in Arabian Gulf: Distribution, Tolerance Thresholds and
946 Threats. *Aquatic Ecosystem Health and Management*, 15(1), 73-83, 2012.
- 947 Ferguson, R. L. and Wood, L. L.: Mapping Submerged Aquatic Vegetation in North Carolina with Conventional
948 Aerial Photography. Federal Coastal Wetland Mapping Programs, National Ocean Pollution Policy Board's
949 Habitat Loss and Modification Working Group. Biological Report, 90(18), pp. 125 – 132. Also available in web:
950 <https://apps.dtic.mil/sti/pdfs/ADA322827.pdf#page=123>, 1990.
- 951 Flood, N.: Comparing Sentinel-2A and Landsat 7 and 8 Using Surface Reflectance over Australia. *Remote Sensing*,
952 9, 659, 2017. DOI: 10.3390/rs9070659, 2017.
- 953 Fourqurean, J. W., Duarte, C. M., Kennedy, H., Marbà, N., Holmer, M., Mateo, M. A., Apostolaki, E. T., Kendrick,
954 G. A., Krause-Jensen, D., McGlathery, K. D. and Serrano, O.: Seagrass ecosystems as a globally significant carbon
955 stock. *Nature Geoscience*, 5(7), 505–509, 2012.
- 956 Fyfe, S. K.: Spatial and temporal variation in spectral reflectance: Are seagrass species spectrally distinct? *Limnology*
957 and *Oceanography*, 48(1, part 2), 464–479. http://dx.doi.org/10.4319/lo.2003.48.1_part_2.0464, 2003.
- 958 Gascon, F., Bouzinac, C., Thépaut, O., Jung, M., Francesconi, B., Louis, J., Lonjou, V., Lafrance, B., Massera, S.,
959 Gaudel-Vacaresse, A., Languille, F., Alhammoud, B., Viallefont, F., Pflug, B., Bieniarz, J., Clerc, S., Pessiot, L.,
960 Trémas, T., Cadau, E., De Bonis, R., Isola, C., Martimort, P. and Fernandez, V.: Copernicus Sentinel-2A
961 Calibration and Products Validation Status. *Remote Sensing*, 9, 584. <https://doi.org/10.3390/rs9060584>, 2017.
- 962 Gitelson, A. A., Kaufman, Y. J., Stark, R. and Rundquist, D.: Novel algorithms for remote estimation of vegetation
963 fraction. *Remote Sensing of Environment*, 80, 76–87, 2002a.
- 964 Gitelson, A. A., Stark, R., Grits, U., Rundquist, D., Kaufman, Y. J. and Derry, D.: Vegetation and soil lines in visible
965 spectral space: a concept and technique for remote estimation of vegetation fraction. *Int. Journal of Remote*
966 *Sensing*, 23(13), 2537–2562, 2002b.
- 967 Green, E. P. and Short, F.: World atlas of seagrasses. Prepared by the UIMEP World Conservation Monitoring Centre.
968 University of California Press, Berkeley, USA, Volume 47. Berkeley (California, USA): University of California.
969 <https://doi.org/10.1515/BOT.2004.029>, 2003.
- 970 Grech, A., Chartrand-Miller, K., Erfteimeijer, P., Fonseca, M., McKenzie, L., Rasheed, M. and Coles, R.: A
971 comparison of threats, vulnerabilities and management approaches in global seagrass bioregions. *Environmental*
972 *Research Letters*, 7(2), 024006, 2012.



- 973 Hamel, M. A. and Andréfouët, S.: Using very high resolution remote sensing for the management of coral reef
974 fisheries: review and perspectives. *Marine Pollution Bulletin*, 60(9),1397-405. DOI:
975 10.1016/j.marpolbul.2010.07.002. Epub 2010 Jul 24, 2010.
- 976 Hashim, M., Misbari, S., Yahya, N. N., Ahmad, S., Reba, M. N. and Komatsu, T.: An approach for quantification of
977 submerged seagrass biomass in shallow turbid coastal waters. In *Proceedings of IGARSS, Quebec, Canada*, pp.
978 4439-4442. DOI: 10.1109/IGARSS.2014.6947476, 2014.
- 979 Hedley, J., Roelfsema, C., Koetz, B. and Phinn, S.: Capability of the Sentinel 2 mission for tropical coral reef mapping
980 and coral bleaching detection. *Remote Sensing of Environment*, 120, 145–155, 2012a.
- 981 Hedley, J. D., Roelfsema, C. M., Phinn, S. R. and Mumby, P. J.: Environmental and sensor limitations in optical
982 remote sensing of coral reefs: implications for monitoring and sensor design. *Remote Sensing*, 4, 271-302.
983 <http://dx.doi.org/10.3390/rs4010271>, 2012b.
- 984 Hossain, M. S., Bujang, J. S., Zakaria, M. H. and Hashim, M.: The application of remote sensing to seagrass
985 ecosystems: An overview and future research prospects. *Int. J. Remote Sensing*, 36(1), 61–113, 2014.
- 986 Huang, Z., Turner, B. J., Dury, S. J., Wallis, I. R. and Foley, W. J.: Estimating foliage nitrogen concentration from
987 HYMAP data using continuum removal analysis. *Remote Sensing of Environment*, 93, 18–29, 2004.
- 988 Huete, A. R.: A soil-adjusted vegetation index (SAVI). *Remote Sensing of Environment*, 25, 295-309, 1988.
- 989 Huete, A. R., Didan, K., Miura, T., Rodriguez, E. P., Gao, X. and Ferreira, L. G.: Overview of the radiometric and
990 biophysical performance of the MODIS vegetation indices. *Remote Sensing of Environment*, 83(1), 195-213.
991 [http://dx.doi.org/10.1016/S0034-4257\(02\)00096-2](http://dx.doi.org/10.1016/S0034-4257(02)00096-2), 2002.
- 992 Humood, N.: Human Impacts on Marine Biodiversity: Macrobenthos in Bahrain, Arabian Gulf. Chapter 7 (pp. 109-
993 126) in “The Importance of Biological Interactions in the Study of Biodiversity. Edited by J. LÃ³pez-Pujol, ISBN:
994 978-953- 307-751-2. Published by InTech, 390 pp, 2011.
- 995 Hunt, Jr. E. R., Doraiswamy, P. C., McMurtrey, J. E., Daughtry, C. S. T., Perry, E. M., and Akhmedov, B.: A visible
996 band index for remote sensing leaf chlorophyll content at the canopy scale. *Int. Journal of Applied Earth
997 Observation and Geoinformation*, 21, 103–112, 2013.
- 998 Indayani, A. B., Danoedoro, P., Wicaksono, P., Winarso, G. and Setiawan, K. T.: Spectral Analysis from Absorption
999 and Reflectance of Seagrass Leaves using Trios-Ramses Spectroradiometer in Nusa Lembongan and Pemuteran,
1000 Bali. *Jurnal Penginderaan Jauh dan Pengolahan Data Citra Digital*, 17(2), 103-113.
1001 <http://dx.doi.org/10.30536/j.pjpdcd.2020.v17.a3384>, 2020.
- 1002 Irons, J. R. Dwyer, J. L. and Barsi, J. A.: The next Landsat satellite: the Landsat data continuity mission. *Remote
1003 Sensing of Environment*, 122, 11–21. <https://doi.org/10.1016/j.rse.2011.08.026>, 2012.
- 1004 Jackson, R. D., Pinter, P. J., Paul, J., Reginato, R. J., Robert, J. and Idso, S. B.: *Hand-Held Radiometry. Agricultural
1005 Reviews and Manuals, ARM-W-19; U.S. Department of Agriculture Science and Education Administration:
1006 Phoenix, AZ, USA, 1980.*
- 1007 James, M. E. and Kalluri, S. N. V.: The Pathfinder AVHRR land data set: an improved coarse resolution data set for
1008 terrestrial monitoring. *Int. Journal of Remote Sensing*, 15(17), 3347–3363, 1994.



- 1009 Johnsen, G. and Sakshaug, E.: Biooptical characteristics of PSII and PSI in 33 species (13 pigment groups) of marine
1010 phytoplankton, and the relevance for pulse amplitude-modulated and fast-repetition-rate fluorometry I. *Journal of*
1011 *Phycology*, 43, 1236–1251, 2007.
- 1012 Joyce, K. E., Phinn, S. R. and Roelfsema, C. M.: Live coral cover index testing and application with hyperspectral
1013 airborne image data. *Remote Sensing*, 5(11), 6116–6137. <http://dx.doi.org/10.3390/rs5116116>, 2013.
- 1014 Kibele, J.: Submerged habitats from space: Increasing map production capacity with new methods and software. PhD
1015 Thesis, Institute of Marine Science, the University of Auckland, New-Zeeland, 179 pp, 2017.
- 1016 Kirk, J. T. O.: *Light and photosynthesis in aquatic ecosystems*, 2nd edition. Cambridge university press, 509 pp.
1017 <https://doi.org/10.1017/CBO9780511623370>, 1994.
- 1018 Knight, E. and Kvaran, G.: Landsat-8 operational land imager design, characterization and performance. *Remote*
1019 *Sensing*, 6(11), 10286–10305, 2014.
- 1020 Knudby, A. and Nordlund, L.: Remote sensing of seagrasses in a patchy multi-species environment. *Int. Journal of*
1021 *Remote Sensing*, 32(8), 2227–2244, 2011.
- 1022 Kokaly, R. F., Despain, D. G., Clark, R. N. and Livo, K. E.: Mapping vegetation in Yellowstone National Park using
1023 spectral feature analysis of AVIRIS data. *Remote Sensing of Environment*, 84, 437–456, 2003.
- 1024 Komatsu, T., Hashim, M., Nurdin, N., Noiraksar, T., Prathep, A., Stankovic, M., Hoang-Son, T. P., Thu, P. M., Luong,
1025 C. V., Wouthyzen, S., Phauk, S., Muslim, A. M., Yahya, N. N., Terauchi, G., Sagawa, T. and Ken-ichi
1026 Hayashizaki, K.-H.: Practical mapping methods of seagrass beds by satellite remote sensing and ground trothing.
1027 *Coastal Marine Science*, 43(1), 1–25, 2020.
- 1028 Konstantinos, T., Spyridon, C. S., Apostolos, P. and Nikolaos, S.: The use of Sentinel-2 imagery for seagrass mapping:
1029 Kalloni Gulf (Lesvos Island, Greece) case study. *Proceedings of the SPIE, Volume 9688, Fourth International*
1030 *Conference on Remote Sensing and Geoinformation of the Environment (RSCy2016)*, 96881F.
1031 [Doi:10.1117/12.2242887](https://doi.org/10.1117/12.2242887), <http://dx.doi.org/10.1117/12.2242887>, 2016.
- 1032 Kovacs, E., Roelfsema, C., Lyons, M., Zhao, S. and Phinn, S.: Seagrass habitat mapping: how do Landsat 8 OLI,
1033 Sentinel-2, ZY-3A, and Worldview-3 perform? *Remote Sensing Letters*, 9(7), 686–695, 2018.
- 1034 Larkum, A. W. D., Orth, R. J. and Duarte, C. M.: Seagrasses: Biology, ecology and conservation. *Seagrasses: Biology,*
1035 *Ecology and Conservation*. <https://doi.org/10.1007/978-1-4020-2983-7>, 2006.
- 1036 Leleu, K., Alban, F., Pelletier, D., Charbonnel, E., Letourneur, Y. and Boudouresque, C.F.: Fishers' perceptions as
1037 indicators of the performance of Marine Protected Areas (MPAs). *Marine Policy*, 36(2), 414–422.
1038 <https://doi.org/10.1016/j.marpol.2011.06.002>, 2012.
- 1039 Li, J. and Chen, B.: Global Revisit Interval Analysis of Landsat-8 -9 and Sentinel-2A-2B Data for Terrestrial
1040 Monitoring. *Sensors*, 20, 6631. <https://doi.org/10.3390/s20226631>, 2020.
- 1041 Li, J. and Roy, D. P.: A Global Analysis of Sentinel-2A, Sentinel-2B and Landsat-8 Data Revisit Intervals and
1042 Implications for Terrestrial Monitoring. *Remote Sensing*, 9, 902. DOI: 10.3390/rs9090902, 2017.
- 1043 Li, S., Ganguly, S., Dungan, J. L., Wang, W. L. and Nemani, R. R.: Sentinel-2 MSI Radiometric Characterization and
1044 Cross-Calibration with Landsat-8 OLI. *Advances in Remote Sensing*, 6, 147–159. DOI : 10.4236/ars.2017.62011.,
1045 2017.



- 1046 Li, R., Liu, J.-K., Sukcharoenpong, A., Yuan, J., Zhu, H. and Zhang, S.: A Systematic Approach toward Detection of
1047 Seagrass Patches from Hyperspectral Imagery, *Marine Geodesy*, 35(3), 271-286, 2012.
- 1048 Li, S.: Seagrass Mapping and Human Impact Evaluation Using Remote Sensing Imagery at Core Banks, North
1049 Carolina. Duke University, 2018.
- 1050 Lin, C., Gong, Z. and Zhao, W.: The extraction of wetland hydrophytes types based on medium resolution TM data.
1051 *Shengtai Xuebao/Acta Ecologica Sinica*, 30(23), 6460–6469, 2010.
- 1052 Loveland, T. R. and Dwyer, J. L.: Landsat: Building a strong future. *Remote Sensing of Environment*, 122, 22–29.
1053 <https://doi.org/10.1016/j.rse.2011.09.022>, 2012.
- 1054 Lyimo, L. D.: Carbon sequestration processes in tropical seagrass beds. PhD Thesis, Department of Ecology,
1055 Environment and Plant Sciences, Stockholm University, Sweden, 2016.
- 1056 Lyons M. B., Phinn S. R. and Roelfsema C. M.: Integrating Quickbird Multi-Spectral Satellite and Field Data:
1057 Mapping Bathymetry, Seagrass Cover, Seagrass Species and Change in Moreton Bay, Australia in 2004 and 2007.
1058 *Remote Sensing*, 3, 42-64. doi:<http://dx.doi.org/10.3390/rs3010042>., 2011.
- 1059 Lyons, M. B., Phinn, S. R. and Roelfsema, C. M.: Long term land cover and seagrass mapping using Landsat and
1060 object-based image analysis from 1972 to 2010 in the coastal environment of South East Queensland, Australia.
1061 *ISPRS Journal of Photogrammetry and Remote Sensing*, 71, 34–46, 2012.
- 1062 Lyons, M. B., Roelfsema, C. M., and Phinn, S. R.: Towards understanding temporal and spatial dynamics of seagrass
1063 landscapes using time-series remote sensing. *Estuarine, Coastal and Shelf Science*, 20, 42–53, 2013.
- 1064 Luczkovich, J., Wagner, T., Michalek, J. and Stoffle, R.: Discrimination of coral reefs, seagrass meadows, and sand
1065 bottom types from space: a Dominican Republic case study. *Photogrammetric Engineering and Remote Sensing*,
1066 59(3), 385–389, 1993.
- 1067 Mandanici, E. and Bitelli, G.: Preliminary Comparison of Sentinel-2 and Landsat 8 Imagery for a Combined Use.
1068 *Remote Sensing*, 8, 1014, 2016. DOI:10.3390/rs8121014., 2016.
- 1069 Manevski, K., Manakos, I., Petropoulos, G. P. and Kalaitzidis, C.: Discrimination of common Mediterranean plant
1070 species using field Spectroradiometry. *Int. J. of Applied Earth Observation and Geoinformation*, 13, 922–933,
1071 2011.
- 1072 Marcello, J., Eugenio, F., Martín, J. and Marqués, F.: Seabed Mapping in Coastal Shallow Waters Using High
1073 Resolution Multispectral and Hyperspectral Imagery. *Remote Sensing*, 10, 1208. DOI:10.3390/rs10081208, 2018.
- 1074 Markham, B., Barsi, J., Kvaran, G., Ong, L., Kaita, E., Biggar, S., Czaplá-Myers, J., Mishra, N. and Helder, D.:
1075 Landsat-8 Operational Land Imager Radiometric Calibration and Stability. *Remote Sensing*, 6(12), 12275-12308.
1076 <https://doi.org/10.3390/rs61212275>, 2014.
- 1077 Markham, B., Jenstrom, D., Masek, J. G., Dabney, P., Pedelty, J. A., Barsi, J.A. and Montanaro, M.: Landsat 9: Status
1078 and plans. In *Earth Observing Systems XXI; International Society for Optics and Photonics: San Diego, CA, USA;*
1079 *Volume 9972*, p. 99720G, 2016.
- 1080 Mcfeeters, S. K.: The use of the normalized difference water index (NDWI) in the delineation of open water features.
1081 *Int. Journal of Remote Sensing*, 17, 1425-1432, 1996.



- 1082 Meehan, A. J., Williams, R. J. and Watford, F. A.: Detecting Trends in Seagrass Abundance Using Aerial Photograph
1083 Interpretation: Problems Arising with the Evolution of Mapping Methods. *Estuaries*, 28(3), 462-472, 2005.
- 1084 Mount, R. E.: Rapid monitoring of extent and condition of seagrass habitats with aerial photography “mega-quadrats.
1085 *Journal of Spatial Science*, 52 (1), 105-119, 2007.
- 1086 Morrison, M. A., Lowe, M. L., Grant, C. M., Smith, P. J., Carbines, G., Reed, J., Bury, S. J. and Brown, J. (2014)
1087 Seagrass meadows as biodiversity and productivity hotspots. *New Zealand Aquatic Environment and Biodiversity*,
1088 Report No. 137, 151 pages. <http://www.mpi.govt.nz/news-resources/publications.aspx>, 2014.
- 1089 Mumby, P. J., Green, E. P., Edwards, A. J. and Clark, C. D.: Measurement of Seagrass Standing Crop using Satellite
1090 and Digital Airborne Remote Sensing. *Marine Ecology Progress Series*, 159, 51-60, 1997.
- 1091 NASA (2014) Landsat-8 Instruments. Available online (accessed on 18 March 2021):
1092 http://www.nasa.gov/mission_pages/landsat/spacecraft/index.html, 2014.
- 1093 NASA: Landsat-9 Mission Details. Available online (accessed on 18 March 2021).
1094 <https://landsat.gsfc.nasa.gov/landsat-9/landsat-9-mission-details/>, 2019.
- 1095 NASA: Landsat-9 overview, continuity the legacy - 2021 and beyond. <https://landsat.gsfc.nasa.gov/landsat-9/landsat-9-overview>, 2021
- 1096
- 1097 Neckles, H. A., Kopp, B. S., Peterson, B. J. and Pooler, P. S.: Integrating Scales of Seagrass Monitoring to Meet
1098 Conservation Needs. *Estuaries and Coasts*, 35(1), 23-46, 2012.
- 1099 Novak, A. B and Short, F. T.: Submerged Aquatic Vegetation: Seagrasses. *Encyclopedia of Natural Resources*, 9
1100 pages. DOI: 10.1081/E-ENRW-120047540, 2014.
- 1101 Onuf, C. P.: Seagrasses, dredging and light in Laguna Madre, Texas, U.S.A.: *Estuarine, Coastal and Shelf Science*,
1102 39, 75-91, 1994.
- 1103 Orth, R. J., Carruthers, T. J. B., Dennison, W. C., Duarte, C. M., Fourqurean, J. W., Heck, K. L., Hughes, A. R.,
1104 Kendrick, G. A., Kenworthy, W. J., Olyarnik, S. Short, F. T., Waycott, M. and Williams, S. L.: A Global Crisis
1105 for Seagrass Ecosystems. *Bioscience*, 56(12), 987-996. [https://doi.org/10.1641/0006-3568\(2006\)56\[987:AGCFSE\]2.0.CO;2](https://doi.org/10.1641/0006-3568(2006)56[987:AGCFSE]2.0.CO;2), 2006.
- 1106
- 1107 Pasqualini, V., Pergent-Martini, C., Pergent, G., Agreil, M., Skoufas, G., Sourbes, L. and Tsirika, A.: Use of SPOT 5
1108 for mapping seagrasses: An application to *Posidonia oceanica*. *Remote Sensing of Environment*, 94(1), 39-45,
1109 2005.
- 1110 Pastick, N. J., Wylie, B. K. and Wu, Z.: Spatiotemporal Analysis of Landsat-8 and Sentinel-2 Data to Support
1111 Monitoring of Dryland Ecosystems. *Remote Sensing*, 10, 791. DOI: 10.3390/rs10050791, 2018.
- 1112 Peneva, E., Griffith, J. A. and Carter, G. A.: Seagrass mapping in the northern Gulf of Mexico using airborne
1113 hyperspectral imagery: a comparison of classification methods. *Journal of Coastal Research*, 24(4), 850-856, 2008.
- 1114 Perez, D., Islam, K., Hill, V., Zimmerman, R., Schaeffer, B., Shen, Y. and Li, J.: Quantifying Seagrass Distribution
1115 in Coastal Water with Deep Learning Models. *Remote Sensing*, 12, 1581. DOI:10.3390/rs12101581, 2020.
- 1116 Peterson, B. J. and Fourqurean, J. W.: Large-scale patterns in seagrass (*Thalassia testudinum*) demographics in south
1117 Florida. *Limnology and Oceanography*, 46(5), 1077-1090, 2001.



- 1118 Phinn, S., Roelfsema, C., Dekker, A., Brando, V. and Anstee, J.: Mapping seagrass species, cover and biomass in
1119 shallow waters: An assessment of satellite multispectral and airborne hyper-spectral imaging systems in Moreton
1120 Bay (Australia). *Remote Sensing of Environment*, 112(8), 3413-3425, 2008.
- 1121 Preen, A.: Distribution, abundance and conservation status of dugongs and dolphins in the southern and western
1122 Arabian Gulf. *Biological Conservation*, 118(2), 205-218, 2004.
- 1123 Pu, R., Bell, S., Baggett, L., Meyer, C. and Zhao, Y.: Discrimination of Seagrass Species and Cover Classes with *in*
1124 *situ* Hyperspectral Data. *Journal of Coastal Research*, 28(6), 1330-1344, 2012.
- 1125 Resson, H., Fyfe, S. K., Natarajan, P. and Snrangam, S.: Monitoring Seagrass Health Using Neural Networks.
1126 Proceedings of IGARSS 2003, pp. 1019-1024, 2003.
- 1127 Richardson, A. J. and Wiegand, C. L.: Distinguishing vegetation from soil background information. *Photogrammetric*
1128 *Engineering and Remote Sensing*, 43(12), 1541-1552, 1977.
- 1129 Roelfsema, C. M., Lyons, M., Kovacs, E. M., Maxwell, P., Saunders, M. I., Samper-Villarreal, J. and Phinn, S. R.:
1130 Multi-temporal mapping of seagrass cover, species and biomass: A semi-automated object based image analysis
1131 approach. *Remote Sensing of Environment*, 150, 172–187, 2014.
- 1132 Roelfsema, C. M., Phinn, S. R., Udy, N. and Maxwell, P.: An integrated field and remote sensing approach for
1133 mapping seagrass cover, Moreton Bay, Australia. *Journal of Spatial Science*, 54(1), 45–62.
1134 <https://doi.org/10.1080/14498596.2009.9635166>, 2009.
- 1135 Rouse, J. W., Haas, R. W., Schell, J. A., Deering, D. W., Harlan, J. C. (1974) Monitoring the vernal advancement and
1136 retrogradation (Greenwave effect) of natural vegetation. NASA/GSFC Type-III Final Report, Greenbelt,
1137 Maryland, U.S.A., 164 pp, 1974.
- 1138 Roy, D. P., Li, J., Zhang, H. K., Yan, L., Huang, H. and Li, Z.: Examination of Sentinel-2A multi-spectral instrument
1139 (MSI) reflectance anisotropy and the suitability of a general method to normalize MSI reflectance to nadir BRDF
1140 adjusted reflectance. *Remote Sensing of Environment*, 199, 25-38. <https://doi.org/10.1016/j.rse.2017.06.019>,
1141 2017.
- 1142 Roy, D., Zhang, H., Ju, J., Gomez-Dans, J., Lewis, P., Schaaf, C., Sun, Q., Li, J., Huang, H. and Kovalskyy, V.: A
1143 general method to normalize Landsat reflectance data to nadir BRDF adjusted reflectance. *Remote Sensing of*
1144 *Environment*, 176, 255–271. <https://doi.org/10.1016/j.rse.2016.01.023>, 2016.
- 1145 Roy, D. P., Wulder, M. A., Loveland, T. R., Woodcock, C. E., Allen, R. G., Anderson, M. C., Helder, D., Irons, J. R.,
1146 Johnson, D. M., Kennedy, R., Scambos, T. A., Schaaf, C. B., Schott, J. R., Sheng, Y., Vermote, E. F., Belward, A.
1147 S., Bindschadler, R., Cohen, W. B., Gao, F., Hipple, J. D., Hostert, P., Huntington, J., Justice, C. O., Kilic, A.,
1148 Kovalskyy, V., Lee, Z. P., Lymburner, L., Masek, J. G., McCorkel, J., Shuai, Y., Trezza, R., Vogelmann, J.,
1149 Wynne, R. H. and Zhu, Z.: Landsat-8: science and product vision for terrestrial global change research. *Remote*
1150 *Sensing of Environment*, 145, 154–172. <https://doi.org/10.1016/j.rse.2014.02.001>, 2014.
- 1151 Saarman, E., Gleason, M., Ugoretz, J., Airamé, S., Carr, M., Fox, E., Frimodig, A., Mason, T. and Vasques, J.: The
1152 role of science in supporting marine protected area network planning and design in California, *Ocean and Coastal*
1153 *Management*, 74, 45-56. <https://doi.org/10.1016/j.ocecoaman.2012.08.021>, 2013.



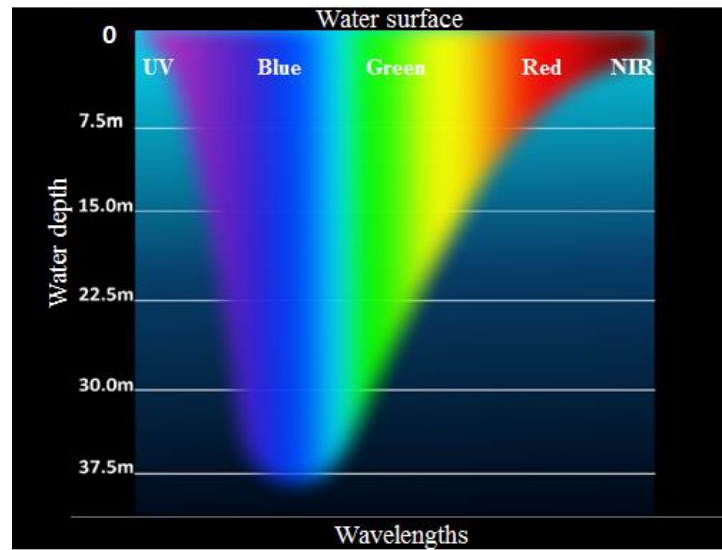
- 1154 Sandmeier, St., Muller, Ch., Hosgood, B. and Andreoli, G.: Sensitivity Analysis and quality Assessment of Laboratory
1155 BRDF Data. *Remote Sensing of Environment*, 64, 176-191, 1998.
- 1156 Shapiro, A. C. and Rohmann, S. O.: Mapping changes in submerged aquatic vegetation using Landsat imagery and
1157 benthic habitat data: Coral reef ecosystem monitoring in Vieques Sound between 1985 and 2000. *Bulletin of*
1158 *Marine Science*, 79(2), 375–388, 2006.
- 1159 Short, F. T. and Wyllie-Echeverria, S.: Natural and human-induced disturbance of seagrasses. *Environ. Conserv.*, 23,
1160 17-27, 1996.
- 1161 Short, F. T. and Coles, R.: *Global Seagrass Research Methods*. Elsevier Publishing, The Netherlands, 482 pp, 2001.
- 1162 Short, F. T., Polidoro, B., Livingstone, S. R., Carpenter, K. E., Bandeira, S., Bujang, J. S., Calumpong, H. P.,
1163 Carruthers, T. J. B., Coles, R. G., Dennison, W. C., Erftemeijer, P. L. A., Fortes, M. D., Freeman, A. S., Jagtap,
1164 T. G., Kamal-Abu-Hena, M., Kendrick, G. A., Kenworthy, W. J., La-Nafie, Y. A., Nasution, I. M., Orth, R. J.,
1165 Prathep, A., Sanciangco, J. C., Tussenbroek, B. V., Vergara, S. G., Waycott, M. W. and Zieman, J. C.: Extinction
1166 risk assessment of the world's seagrass species. *Biological Conservation*, 144(7), 1961–1971.
1167 <https://doi.org/10.1016/j.biocon.2011.04.010>, 2011.
- 1168 Silva, T. S. F., Costa, M. P. F., Melack, J. M., and Novo, E. M. L. M.: Remote sensing of aquatic vegetation: Theory
1169 and applications. *Environmental Monitoring and Assessment*, 140(1-3), 131-145. [https://doi.org/10.1007/s10661-](https://doi.org/10.1007/s10661-007-9855-3)
1170 [007-9855-3](https://doi.org/10.1007/s10661-007-9855-3), 2008.
- 1171 Skakun, S., Roger, J.-C., Vermote, E. F., Masek, J. G. and Justice, C. O.: Automatic sub-pixel co-registration of
1172 Landsat-8 Operational Land Imager and Sentinel-2A Multi-Spectral Instrument images using phase correlation
1173 and machine learning based mapping. *Int. J. of Digital Earth*, 10(12), 1253-1269.
1174 <http://dx.doi.org/10.1080/17538947.2017.1304586>, 2017.
- 1175 Slater, P. N.: *Remote Sensing - Optics and Optical System*. Addison-Wesley, reading, MA, 575 pp. 1980.
- 1176 Teillet, P. M. and Santer, R.: Terrain Elevation and Sensor Altitude Dependence in a Semi-Analytical Atmospheric
1177 Code". *Canadian J. of Remote Sensing*, 17, 36-44, 1991.
- 1178 Thakur, Y. et al.: Sea Turtles. Chapter 9, pp. 165–177. In *Marine Environment and Resources of Abu Dhabi*, edited
1179 by T.Z. Al-Abdessalam, published by Environment Agency of Abu-Dhabi, UAE, 255 pp, 2007.
- 1180 Thorhaug, A., Richardson, A. D. and Berlyn, G. P.: Spectral reflectance of the seagrasses: *Thalassia testudinum*,
1181 *Halodule wrightii*, *Syringodium filiforme* and five marine algae. *Int. Journal of Remote Sensing*, 28(7), 1487–
1182 1501, 2007.
- 1183 Traganos, D.: Development of seagrass monitoring techniques using remote sensing data. PhD Thesis, Osnabrück
1184 University, [Osnabrück](https://www.osnabrueck.de) in Lower Saxony, Germany, 199 pp, 2020.
- 1185 Uhrin, A. V. and Townsend, P. H.: Improved Seagrass Mapping Using Linear Spectral Unmixing of Aerial
1186 Photographs. *Estuarine, Coastal and Shelf Science*, 171, 11-22, 2016.
- 1187 Umamaheswari, R., Ramachandran, S. and Nobi, E. P.: Mapping the extend of seagrass meadows of Gulf of Mannar
1188 Biosphere Reserve, India using IRS ID satellite imagery. *Int. Journal of Biodiversity and Conservation*, 1(5), 187-
1189 193, 2009.



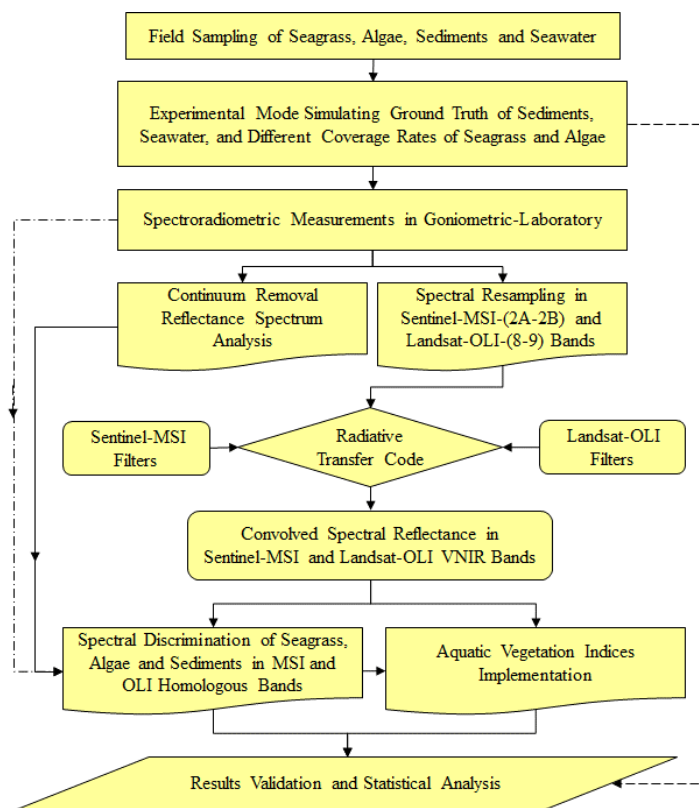
- 1190 Van-Der-Meera, F.: Analysis of spectral absorption features in hyperspectral imagery. *Int. J. Appl. Earth Observation*
1191 and *Geoinformation*, 5, 55–68, 2004.
- 1192 Van der Werff, H. and Van der Meer, F.: Sentinel-2A MSI and Landsat 8 OLI Provide Data Continuity for Geological
1193 Remote Sensing. *Remote Sensing*, 8, 883. <https://doi.org/10.3390/rs8110883>, 2016.
- 1194 Vermote, E., Justice, C., Claverie, M. and Franch, B.: Preliminary analysis of the performance of the Landsat 8/OLI
1195 land surface reflectance product. *Remote Sensing of Environment*, 185(2), 46–56.
1196 DOI: 10.1016/j.rse.2016.04.008, 2016.
- 1197 Villa, P., Bresciani, M., Braga, F. and Bolpagni, R.: Comparative Assessment of Broadband Vegetation Indices over
1198 Aquatic Vegetation. *IEEE Journal of Selected Topics in Applied Earth Observations and Remote Sensing*, 7(7),
1199 3117-3127, 2014.
- 1200 Villa, P., Mariano Bresciani, M., Braga, F. and Bolpagni, R.: Mapping Aquatic Vegetation through Remote Sensing
1201 Data: A Comparison of Vegetation Indices Performances. 6th EARSeL Workshop on Remote S. of the Coastal
1202 Zone, 7-8 June 2013, Matera, Italy, pp. 10-15, 2013.
- 1203 Vuolo, F., Zóltak, M., Pipitone, C., Zappa, L., Wennig, H., Immitzer, M., Weiss, M., Baret, F. and Atzberger, C.: Data
1204 service platform for Sentinel-2 surface reflectance and value-added products: System use and examples. *Remote*
1205 *Sensing*, 8, 938, 2016.
- 1206 Wabnitz, C. C., Andréfouët, S., Torres-Pulliza, D., Muller-Karger, F. E. and Kramer, P. A.: Regional-scale seagrass
1207 habitat mapping in the Wider Caribbean region using Landsat sensors: Applications to conservation and ecology.
1208 *Remote Sensing of Environment*, 12(8), 3455-3467, 2008.
- 1209 Warren, C., Dupont, J., Abdel-Moati, M., Hobeichi, S., Palandro, D. and Purkis, S.: Remote sensing of Qatar nearshore
1210 habitats with perspectives for coastal management. *Marine Pollution Bulletin*, 105(2), 641-653.
1211 <https://doi.org/10.1016/j.marpolbul.2015.11.036>, 2016.
- 1212 Waycott, M., Duarte, C. M., Carruthers, T. J. B., Orth, R. J., Dennison, W. C., Olyarnik, S., Calladine, A.,
1213 Fourqurean, J. W., Heck Jr., K. L., Hughes, A. R., Kendrick, G. A., Kenworthy, W. J., Short, F. T. and Williams,
1214 S. L.: Accelerating loss of seagrasses across the globe threatens coastal ecosystems. *PNAS* July 28,
1215 2009; 106 (30) 12377-12381; www.pnas.org/cgi/doi/10.1073/pnas.0905620106, 2009.
- 1216 Wicaksono, P. and Hafizt, M.: Mapping Seagrass from Space: Addressing the Complexity of Seagrass LAI Mapping,
1217 *European Journal of Remote Sensing*, 46(1), 18-39. <http://dx.doi.org/10.5771/EuJRS20134602>, 2013.
- 1218 Wicaksono, P., Fauzan, M. A., Kumara, I. S. W., Yogyantoro, R. N., Lazuardi, W. and Zhafarina, Z.: Analysis of
1219 reflectance spectra of tropical seagrass species and their value for mapping using multispectral satellite images.
1220 *Int. Journal of Remote Sensing*, 40(23), 8955-8977. DOI: 10.1080/01431161.2019.1624866, 2019.
- 1221 Wicaksono, P., Kumara, I. S., Kamal, M., Fauzan, A. M., Zhafarina, Z., Nurswantoro, D. A. and Yogyantoro, R. N.:
1222 Multispectral Resampling of Seagrass Species Spectra: WorldView-2, Quickbird, Sentinel-2A, ASTER VNIR,
1223 and Landsat 8 OLI. The 5th Geoinformation Science Symposium 2017 (GSS 2017). *IOP Conf. Series: Earth and*
1224 *Environmental Science*, 98(2017), 012039. DOI:10.1088/1755-1315/98/1/012039, 2017.
- 1225 Willmott, C.J.: Some comments on the evaluation of model performance. *Bull. Am. Meteorol. Soc.*, 63, 1309-1313,
1226 1982.



- 1227 Wood, J. S.: Hyperspectral analysis of seagrass in Redfish Bay, Texas. Ph.D. Thesis, Texas A&M University-Corpus
1228 Christi, Corpus Christi, Texas (USA), 141 pp, 2012.
- 1229 Wulder, M. A., Hilker, T., White, J. C., Coops, N. C., Masek, J. G., Pflugmacher, D. and Crevier, Y.: Virtual
1230 constellations for global terrestrial monitoring. *Remote Sensing of Environment*, 170, 62–76.
1231 <https://doi.org/10.1016/j.rse.2015.09.001>, 2015.
- 1232 Yan, L., Roy, D.P., Li, Z., Zhang, H.K. and Huang, H.: Sentinel-2A multi-temporal misregistration characterization
1233 and an orbit-based sub-pixel registration methodology. *Remote Sensing of Environment*, 215, 495-506.
1234 <https://doi.org/10.1016/j.rse.2018.04.021>, 2018.
- 1235 Yang, D. and Yang, C.: Seagrass Distribution in China with Satellite Remote Sensing. Chapter 4 in *Remote Sensing*
1236 *of Planet Earth*, edited by Yann Chemin, pp. 75-94. ISBN: 978-953-307-919-6, InTech. Available from:
1237 [http://www.intechopen.com/books/remote-sensing-of-planet-earth/seagrass-distribution-in-china-with-](http://www.intechopen.com/books/remote-sensing-of-planet-earth/seagrass-distribution-in-china-with-remotesensing)
1238 [remotesensing](http://www.intechopen.com/books/remote-sensing-of-planet-earth/seagrass-distribution-in-china-with-remotesensing), 2012.
- 1239 Yang, D. and Yang, C.: Detection of seagrass distribution changes from 1991 to 2006 in Xincun Bay, Hainan, with
1240 satellite remote sensing. *Sensors*, 9(2), 830-844, 2009.
- 1241 Zhang, H. K. and Roy, D. P.: Computationally inexpensive Landsat-8 operational land imager (OLI) pan-sharpening.
1242 *Remote Sensing*, 8 (3), 180, 2016.
- 1243 Zhang, H. K., Roy, D. P., Yan, L., Li, Z., Huang, H., Vermote, E., Skakun, S. and Roger, J. C.: Characterization of
1244 Sentinel-2A and Landsat-8 top of atmosphere, surface, and nadir BRDF adjusted reflectance and NDVI
1245 differences. *Remote Sensing of Environment*, 215, 482-494. <https://doi.org/10.1016/j.rse.2018.04.031>, 2018.
- 1246 Zhao, D., Ly, M., Jiang, H., Cai, Y., Xu, D. and An, S.: Spatio-Temporal Variability of Aquatic Vegetation in Taihu
1247 Lake over the Past 30 Years. *PLoS ONE*, 8(6), 6–12. <https://doi.org/10.1371/journal.pone.0066365>, 2013.
- 1248 Zoffoli, M. L., Gernez, P., Rosa, P., Le-Bris, A., Brando, V. E., Barille, A.-L., Harin, N., Peters, S., Poser, K., Spaias,
1249 L., Peralta, G. and Barille, L.: Sentinel-2 remote sensing of *Zostera noltei*-dominated intertidal seagrass meadows.
1250 *Remote Sensing of Environment*, 251, 112020, 2020.
- 1251 Zorrilla, N. A., Vantrepotte, V., Ngoc, D.-D., Huybrechts, N. and Gardel, A.: Automated SWIR based empirical sun
1252 glint correction of Landsat 8-OLI data over coastal turbid water. *Optics Express*, 27(8), A294-A318.
1253 <https://doi.org/10.1364/OE.27.00A294>, 2019.
- 1254
1255
1256
1257
1258



1259
1260 **Figure 1.** Vertical penetration of electromagnetic spectrum in shallow water (adapted from: Morris, 2019),
1261 https://commons.wikimedia.org/wiki/Category:Visible_spectrum_illustrations)
1262
1263
1264
1265
1266
1267
1268



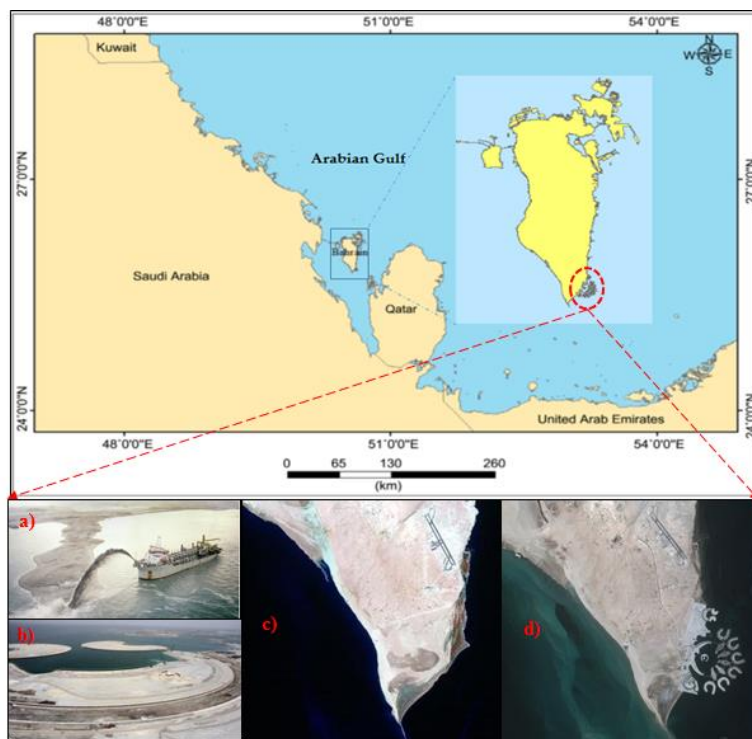
1269

1270 **Figure 2.** Methodology Flowchart

1271

1272

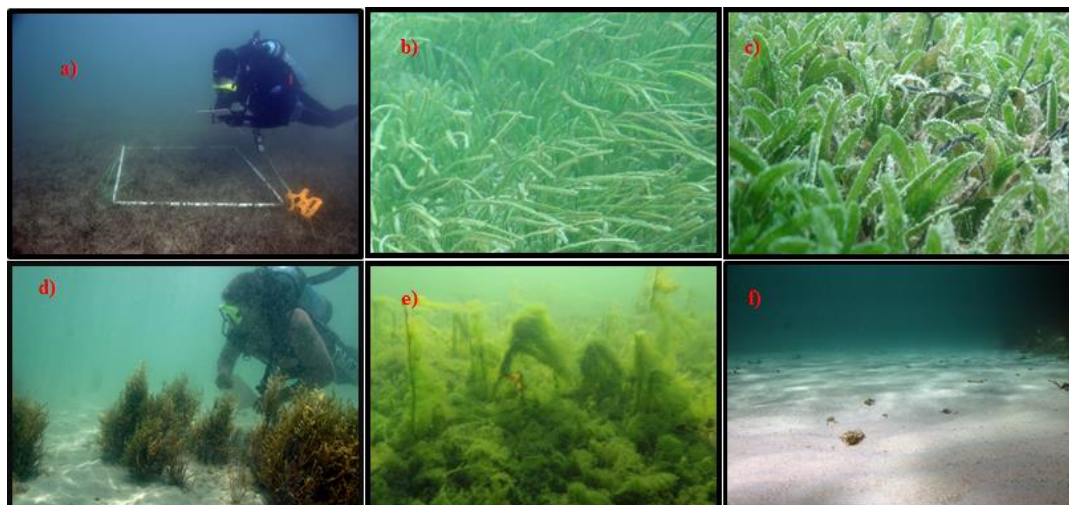
1273



1274

1275 **Figure 3.** Study site (Kingdom of Bahrain), photos illustrating dredging operations (a and b), and satellite images of
1276 the south part of Bahrain before (c) and after (d) artificial islands construction.

1277



1278

1279 **Figure 4.** Diver for sampling operation (a), and underwater photos of the considered seagrass and algae species: HU
1280 (b), HS (c), BA (d), GA (e), and bright sediments (f).



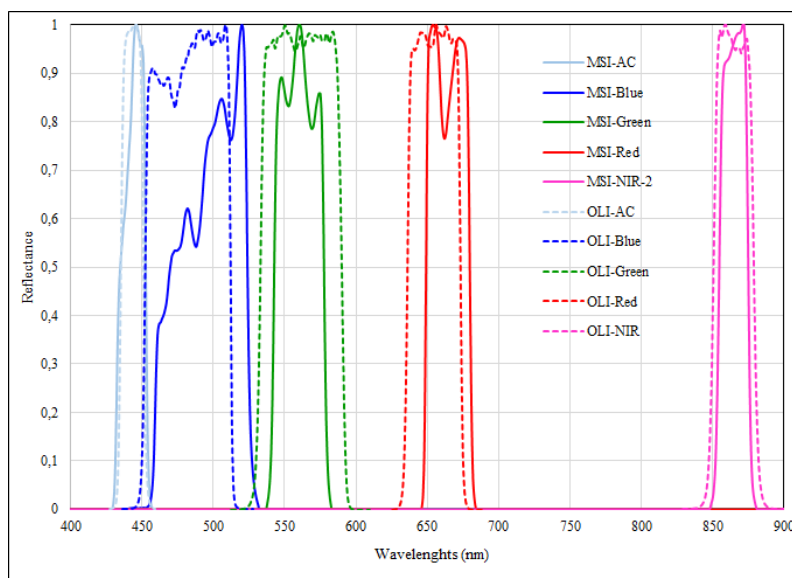
1281



1282

1283 **Figure 5:** Dark Goniometric-Laboratory for ASD measurements.

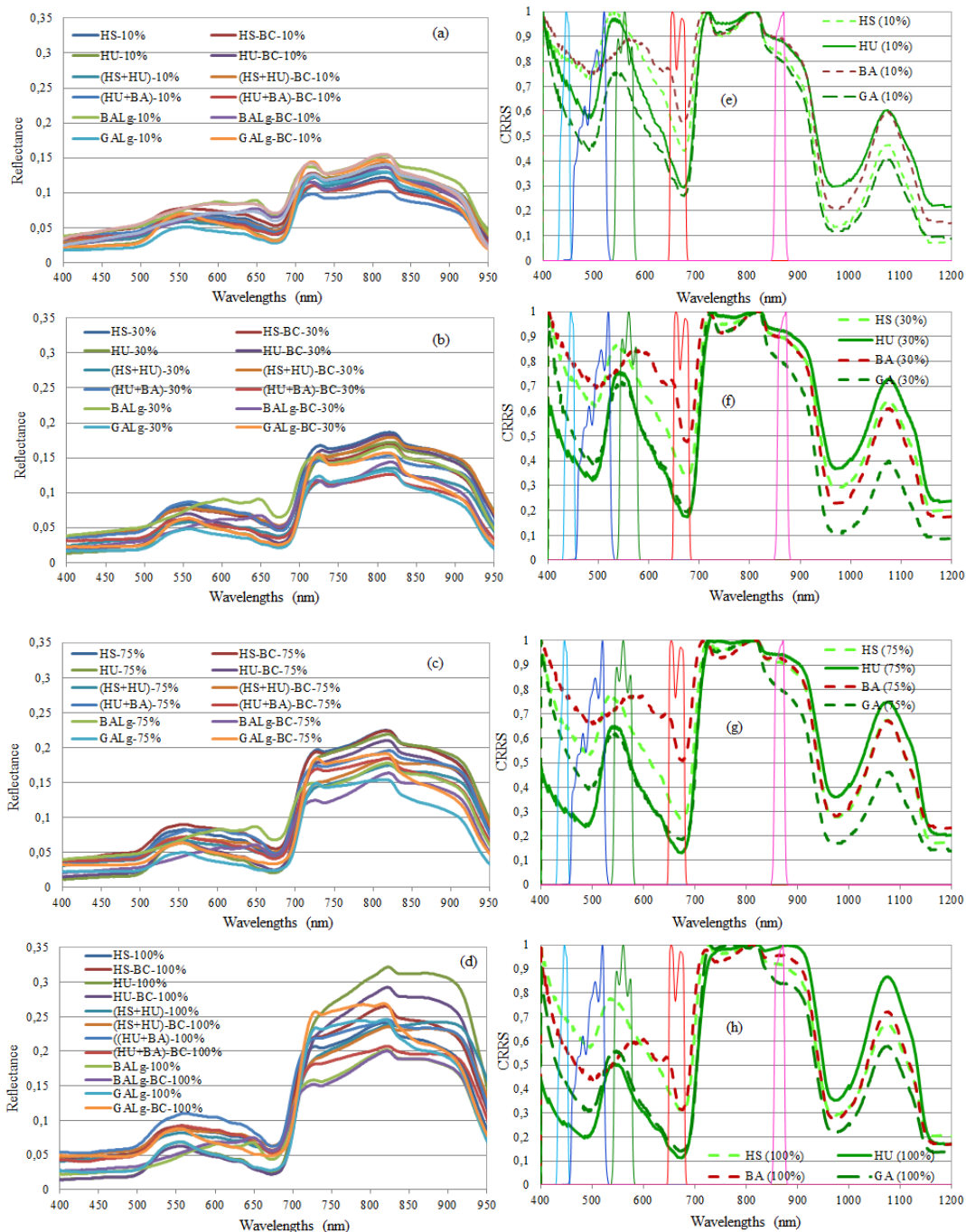
1284



1285

1286 **Figure 6.** Sentinel-MSI and Landsat-OLI relative spectral response profiles characterizing the filters of each spectral
1287 band in the VNIR.

1288



1289

1290

1291

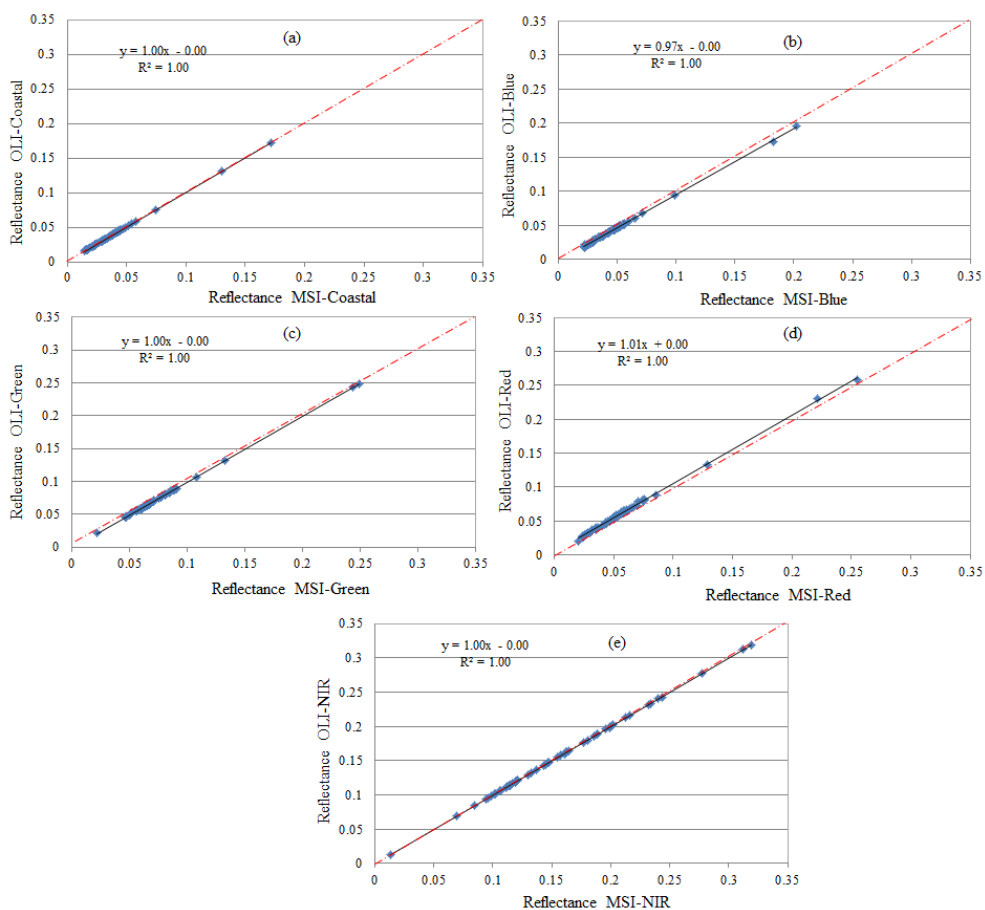
Figure 7. Spectral signatures of seagrass and algae samples at different coverage rates and CRRS transformations.

1292



1293

1294



1295

1296 **Figure 8.** Scatter-plots of reflectances sampled and convolved in MSI and OLI homologous spectral bands.

1297

1298

1299

1300

1301

1302

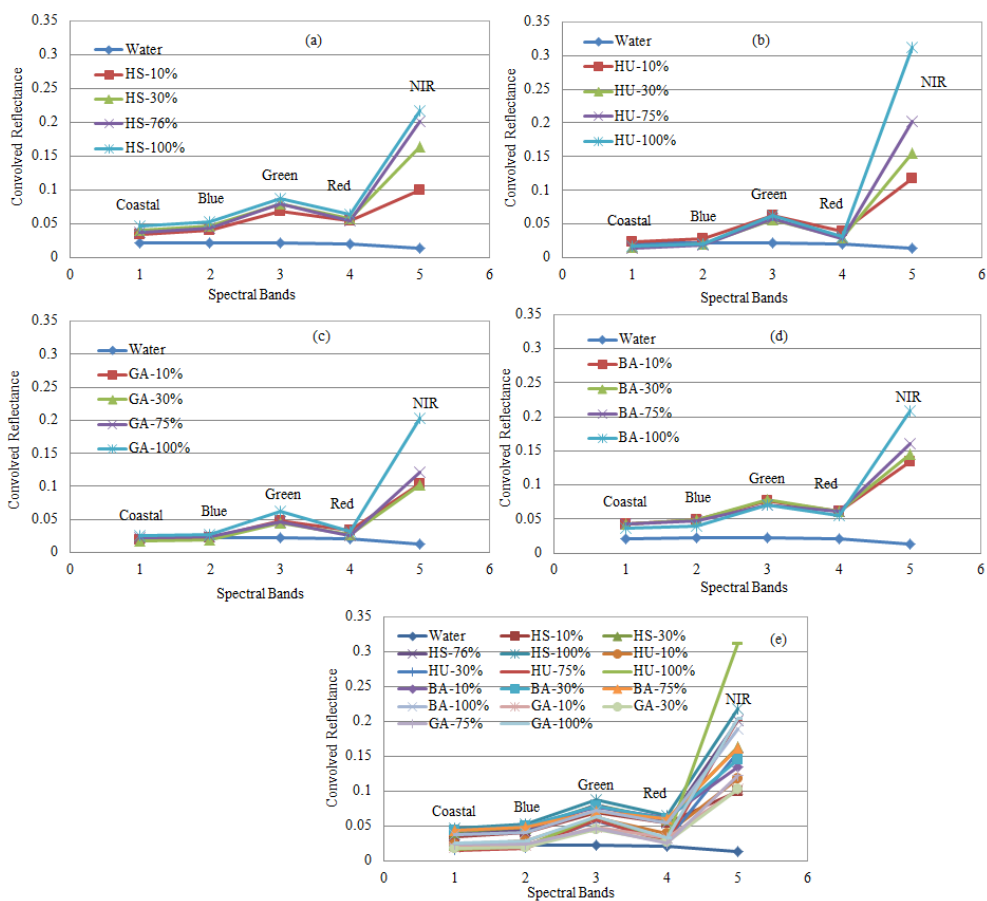
1303

1304



1305

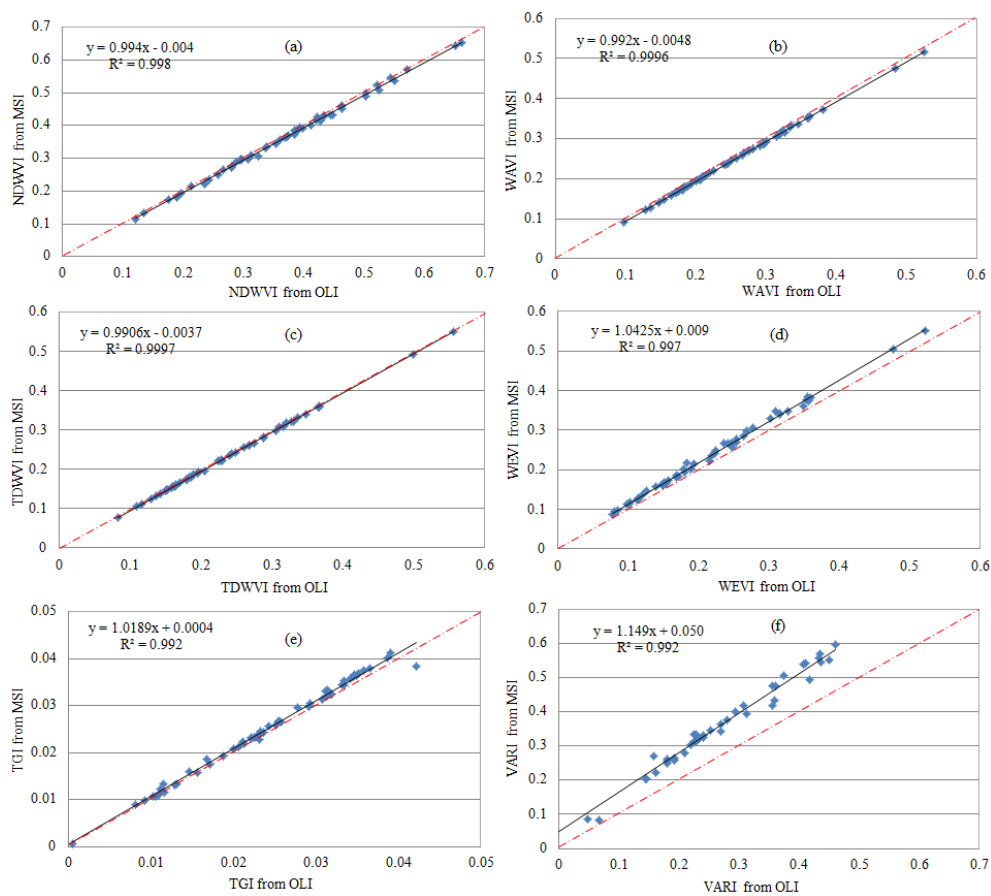
1306



1307

1308 **Figure 9.** Seagrass, algae, and seawater reflectances resampled and convolved in VNIR bands of Sentinel-MSI (or
1309 Landsat-OLI): HS (a), HU (b), GA (c), BA (d), and all samples (e).

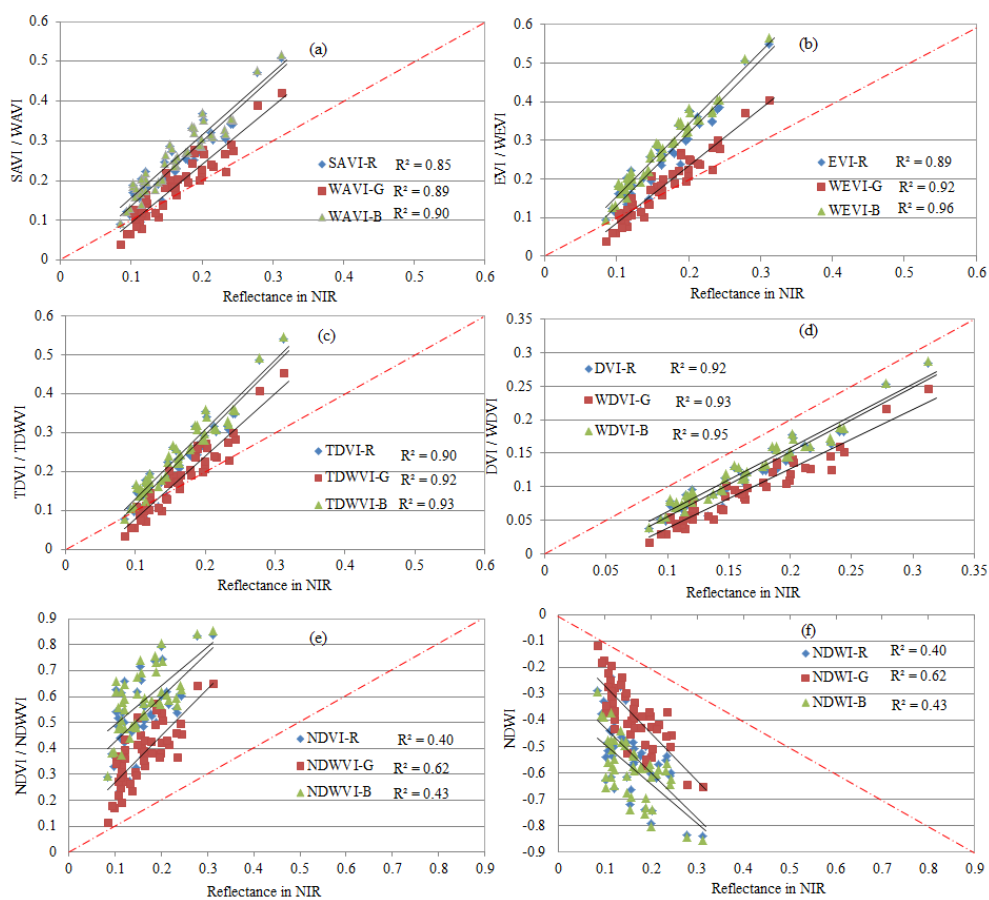
1310



1311

1312 **Figure 10.** Scatter-plots of homologous WVI derived from MSI and OLI simulated data.

1313



1314

1315 **Figure 11.** Linear regressions ($p < 0.05$) between WVI and reflectance in NIR considering all samples, and integrating
 1316 the red, green, and blue bands.

1317

1318 **Table 1.** The Sentinel-MSI and Landsat-OLI effective bandwidths and characteristics (λ = wavelength, SNR = signal
 1319 to noise ratio, $L_{ref}(\lambda)$ = reference radiance, $E_0(\lambda)$ = Extra-atmospheric irradiance,).

Spectral Bands	Sentinel-MSI					Landsat-OLI				
	λ Centre (nm)	$\Delta\lambda$ (nm)	Pixel Size (m)	SNR	$L_{ref}(\lambda)$ ($w/m^2/Sr/\mu m$)	λ Centre (nm)	$\Delta\lambda$ (nm)	Pixel Size (m)	SNR	$E_0(\lambda)$ ($w/m^2/\mu m$)
Coastal	443	20	60	129	129	443	16	30	130	1895.6
Blue	490	65	10	154	128	482	60	30	130	2004.6
Green	560	35	10	168	128	561	57	30	100	1820.7
Red	655	30	10	142	108	655	38	30	90	1549.4
NIR-2	865	20	20	72	52.5	865	28	30	90	951.2
SWIR-1	1609	85	20	100	4	1609	85	30	100	247.6
SWIR-2	2201	187	20	100	1.5	2201	187	30	100	85.5

1320

1321



1322

1323 **Table 2.** R^2 ($p < 0.05$) between vegetation indices integrating red, blue, and green bands and the reflectances in NIR

1324 for all considered samples, and the RMSD between indices derived from MSI and OLI sensors data.

Index	Used band	R^2	RMSD * in %	Index	Used band	R^2	RMSD * in %	Index	Used band	R^2	RMSD * in %
NDVI	R	0.40	1.0	TDVI	R	0.90	0.3	DVI	R	0.92	0.2
	G	0.63	0.5		G	0.92	0.2		G	0.93	0.1
	B	0.43	1.0		B	0.93	0.2		B	0.95	0.1
SAVI	R	0.85	0.3	EVI	R	0.89	0.9	NDWI	R	0.40	1.0
	G	0.89	0.2		G	0.92	0.3		G	0.63	0.5
	B	0.90	0.2		B	0.96	0.3		B	0.43	1.0
TGI		0.20	0.1	Diff(G-B)		0.63	0.1	VARI		0.63	3.0

1325 * is the RMSD between indices derived from MSI and OLI simulated data. The bold type highlight the significant R^2 .

1326

1327